Numerical Relativity and Astrophysics

Luis Lehner[1] and Frans Pretorius[2]

[1]Perimeter Institute for Theoretical Physics, Waterloo, Ontario N2L 2Y5, Canada; email: llehner@perimeterinstitute.ca

[2]Department of Physics, Princeton University, Princeton, New Jersey 08544; email: fpretori@princeton.edu

Annu. Rev. Astron. Astrophys. 2014. 52:661–94

First published online as a Review in Advance on June 16, 2014

The *Annual Review of Astronomy and Astrophysics* is online at astro.annualreviews.org

This article's doi: 10.1146/annurev-astro-081913-040031

Keywords

black holes, neutron stars, gravitational waves, gamma-ray bursts

Abstract

Throughout the Universe many powerful events are driven by strong gravitational effects that require general relativity to fully describe them. These include compact binary mergers, black hole accretion, and stellar collapse, where velocities can approach the speed of light and extreme gravitational fields ($\Phi_{\rm Newt}/c^2 \simeq 1$) mediate the interactions. Many of these processes trigger emission across a broad range of the electromagnetic spectrum. Compact binaries further source strong gravitational wave emission that could directly be detected in the near future. This feat will open up a gravitational wave window into our Universe and revolutionize our understanding of it. Describing these phenomena requires general relativity, and—where dynamical effects strongly modify gravitational fields—the full Einstein equations coupled to matter sources. Numerical relativity is a field within general relativity concerned with studying such scenarios that cannot be accurately modeled via perturbative or analytical calculations. In this review, we examine results obtained within this discipline, with a focus on its impact in astrophysics.

1. INTRODUCTION

Strong gravitational interactions govern many of the most fascinating astrophysical phenomena and lie behind some of the most spectacular predictions of general relativity, such as black holes and neutron stars. These objects produce extreme gravitational fields and are believed to be responsible for the most energetic events in our Universe. Indeed, models for gamma-ray bursts, quasars, AGNs, pulsars, and a class of ultra-high-energy cosmic rays all peg these still poorly understood compact objects as putative central engines. Observations across the electromagnetic spectra, soon to be combined with gravitational signals produced by merging binaries, should provide important insights into their natures. Of course, such understanding can only be gained by contrasting theoretical models that include all the relevant physics with the full front of observations.

It is important to distinguish two subclasses of strongly gravitating systems. The first is where the self-gravitation of any matter/gas/plasma interacting with a compact object or binary is sufficiently weak such that the gravitational back reaction can be ignored or treated perturbatively. Such systems can be analyzed by studying the dynamics of matter on a given fixed background geometry. Examples include accreting black holes and tidal disruption of main sequence stars by a supermassive black hole. Widely separated compact binary systems also belong to this subclass, and suitable post-Newtonian (PN) expansions can be adopted to account for the slowly varying gravitational field and its effects.

By contrast, the second subclass is where the interaction is strong and can fundamentally affect the gravitational field of the system. In this case, a fully relativistic, self-gravitating study must be performed. To this end the Einstein equations, coupled to any relevant matter fields, must be employed. This task is complex due to the involved nature of Einstein's equations (a nonlinear, strongly coupled system of equations) in which analytical solutions are only known in highly specialized scenarios. Consequently, numerical simulations are required, and the discipline that concentrates on the development and application of numerical solutions of Einstein's equations is known as numerical relativity (NR).

This discipline has, over several decades, steadily progressed to the current epoch in which studies of relevance to astrophysics can now be performed that address questions of fundamental theoretical interest and that make contact with observations. [NR is also being used to address problems in cosmological contexts. Applications that require NR, including bubble collisions (Johnson, Peiris & Lehner 2012; Wainwright et al. 2014), the evolution near the bounce in cyclic models (Garfinkle et al. 2008, Xue et al. 2013), and certain aspects of cosmic string dynamics (Laguna & Garfinkle 1989), are still at either a speculative level or being explored. In contrast, the paradigm applicable to most of present day observational cosmology can effectively be addressed with exact Friedman-Lamaitre-Robison-Walker solutions and perturbations about them, and do not require NR.] Of particular interest, spurred by a hope of imminent gravitational wave observation, are systems capable of producing strong gravitational emission. Detectors include ground-based interferometers, such as LIGO (Laser Interferometer Gravitational-Wave Observatory), VIRGO, and KAGRA (Kamioka Gravitational wave detector) (Abbott et al. 2009, Accadia et al. 2011, Somiya 2012) targeting the $\simeq$10Hz–1 kHz frequency band; a pulsar timing network (see, e.g., Int. Pulsar Timing Array 2013) sensitive to the 300 pHz–100 nHz window; and possible future spaced-based missions [such as NGO (*New Gravitational-Wave Observatory*) or eLISA (*Evolved Laser Interferometer Space Antenna*); see, e.g., Amaro-Seoane et al. 2012] sensitive to $\simeq$10 μHz–0.1 Hz. Compact binary systems, involving black holes or neutron stars, are the most natural sources and have thus been the focus of most recent efforts (see, e.g., Andersson et al. 2013 for a recent overview). In this article, we review the key messages obtained by NR relevant to astrophysics. The discipline is still in the midst of rapid development over an increasing breadth of applications, promising even more exciting future discoveries of astrophysical import.

2. BRIEF REVIEW OF TECHNIQUES, METHODS, AND INFORMATION OBTAINABLE FROM GRAVITATIONAL WAVES

Understanding gravity in highly dynamical/strongly gravitating regimes requires solving Einstein's equations. This provides the metric tensor, g_{ab}, which encodes gravitational effects in geometrical terms. The covariant character of the equations encode the equivalence principle, hence there is no preferred frame of reference to write the particular form of the metric for a given physical geometry. This further implies that the field equations determining g_{ab} do not lend themselves to a well-defined initial value problem unless the spacetime is foliated into a series of surfaces that provide a notion of "time." One can then cast Einstein's equations in a form that provides a recipe to evolve the intrinsic metric of each slice with time in what has been called geometrodynamics. There are several options to carry out this program (see, e.g., the discussion by Lehner 2001), though the most common one is to define these surfaces to be spacelike. This is also most closely related to Newtonian mechanics and, hence, provides useful intuition in astrophysical scenarios; furthermore, with some additional assumptions about the coordinates, the familiar Newtonian potential can easily be extracted from the metric for weakly gravitating systems. Current efforts most commonly employ one of two particular reformulations of Einstein's equations: the generalized harmonic or the BSSN (Barmgarte-Shapiro-Shibata-Nakamura) formulations (for a recent review, see Sarbach & Tiglio 2012). These equations are hyperbolic with characteristics given by the speed of light (regardless of the state of the system, as opposed to the familiar case of hydrodynamics in which perturbations propagate with speeds tied to the state of the fluid). When coupling in matter sources, the equations of relativistic hydrodynamics (or magnetohydrodynamics) on a dynamical, curved geometry must also be considered. The relevant equations can be expressed in a way fully consistent with standard approaches to integrate the Einstein equations (for a review on this topic, see Font 2008).

With the equations defined, they can be discretized for numerical integration. For the systems considered here, a crucial observation is that simulations must be carried out in full generality. This means that time and spatial variations are equally important, and a disparate range of scales need to be resolved (ranging from at least the size of each compact object, through the scale in which gravitational waves are produced, and to the asymptotic region where they are measured). The associated computational cost is quite high, and typical simulations run on hundreds to thousands of processors for hours to weeks, even when efficient resolution of the relevant spatio-temporal scales can be achieved using (for example) adaptive mesh refinement. It is beyond the scope of this review to describe the techniques employed in detail, though we briefly mention them and point to some relevant literature for further details. [See also a few textbooks on the subject written in recent years by Alcubierre (2008); Bona, Bona-Casas & Palenzuela-Luque (2009); Baumgarte & Shapiro (2010)].

1. *Spatial discretization.* As far as the gravitational field itself is concerned, solutions are generally smooth (except at singularities) provided smooth initial data are defined because the equations of motions are linearly degenerate (i.e., do not induce shocks from smooth initial data). High-order finite difference approximations (e.g., Gustafsson, Kreiss & Oliger 1995) or spectral decompositions (e.g., Boyd 1989, Grandclement & Novak 2009) allow for a high degree of accuracy. When matter and therefore the hydrodynamic equations are involved, finite volume methods and high-resolution shock capturing schemes can be used to determine the future evolution of the fluid variables (e.g., LeVeque 1992).
2. *Time integration.* The method of lines can be straightforwardly implemented once spatial derivatives are computed.

3. *Constraint enforcement.* For systems of interest, several constraints are typically involved. Those coming from Einstein's equations themselves are a nonlinear coupled set of partial differential equations. In general scenarios, these constraints are difficult to enforce directly; instead, a strategy of constraint damping is adopted, whereby the equations of motion are modified in a suitable manner via the addition of constraints. The resulting system is thus not different from the initial one when the constraints are satisfied, otherwise the numerical evolution should damp these violations as time progresses. This desirable behavior can be rigorously shown to hold in perturbations off flat spacetime (Brodbeck et al. 1999, Gundlach et al. 2005) and also "experimentally" verified in simulations involving black holes and neutron stars (e.g., Pretorius 2005, 2006; Anderson et al. 2008a; Chawla et al. 2010). This technique—whereby the equations are suitably modified to control constraints—has also been extended to other relevant systems of equations. For instance, when considering magnetohydrodynamics or electrodynamics, to control the no-monopole constraint (Neilsen, Hirschmann & Millward 2006; Palenzuela, Lehner & Yoshida 2010).
4. *Mesh structure, resolution, and adaptivity.* As mentioned, several different physical scales need to be resolved. For efficient implementation, techniques like adaptive mesh refinement and multiple patches are in common use (e.g., Berger & Oliger 1984; Schnetter, Hawley & Hawke 2004; Lehner, Reula & Tiglio 2005; Lehner, Liebling & Reula 2006; Duez et al. 2008; East, Pretorius & Stephens 2012b).
5. *Parallelization.* The equations involved are of hyperbolic type, and they lend themselves naturally to a relatively straightforward parallelization. Several computational infrastructures have been developed for NR purposes, e.g., BAM, Cactus (**http://www.cactuscode.org**) and the Einstein Toolkit (Löffler et al. 2011), HAD (**http://had.liu.edu**), Whisky, and SACRA (Baiotti, Shibata & Yamamoto 2010).

3. BRIEF DESCRIPTION OF THE DYNAMICS OF A BINARY SYSTEM

Here we review salient properties of the early phase of binary evolution in general relativity to set the stage for subsequent discussion of the nonlinear regime uncovered by numerical simulations. For further details, the interested reader can consult Hughes (2009).

An isolated compact binary evolves owing to the emission of gravitational waves, and consequently a bound system will eventually merge. The end state of compact binary mergers (i.e., binary black holes, black hole–neutron star binaries, and all except the least massive binary neutron stars) is a single Kerr black hole (provided cosmic censorship holds, and there are no indications yet that it fails for mergers in four-dimensional, asymptotically flat spacetime). At large separations, in which the local velocity of each object in the binary is small (relative to the speed of light c), a PN expansion (e.g., Blanchet 2002), where objects are taken as point-particles without internal dynamics, suffices to accurately describe the system. As the orbit shrinks, the faithfulness of such an expansion decreases as velocities become $O(c)$. If either compact object is a neutron star tidal effects may be important; these can be modeled within the PN framework, though again the accuracy of the expansion degrades approaching tidal disruption, which can occur near merger for stellar mass binaries. During this late stage of inspiral, a full numerical solution must be employed to obtain an accurate description of the dynamics of the geometry and matter. Once a single black hole forms, very shortly afterward (on the order of a few light-crossing times of the Schwarzschild radius) the spacetime can accurately be modeled by black hole perturbation theory, and to a good approximation the matter can be evolved on a stationary black hole background. In the standard jargon of the field, the three different stages just described are often referred to as the PN inspiral, nonlinear, and ringdown stages.

The nonlinear phase can further be subdivided into a late inspiral, plunge, and early post-merger epoch (see, e.g., Buonanno, Cook & Pretorius 2007; Buonanno, Kidder & Lehner 2008). In the first subphase the binary is still in an orbit; though velocities are high, the orbital frequency quickly sweeps upward, and neutron star tidal dynamics can become relevant (if the companion is a neutron star or black hole with mass $\lesssim 20\,M_\odot$). The second subphase refers to a rapid increase in the magnitude of the inward radial velocity leading to merger. The plunge is related to the phenomenon of the innermost stable circular orbit (ISCO) of a black hole and is, thus, most apparent in a high-mass-ratio compact binary. The last subphase begins when either a black hole or a hypermassive neutron star forms and lasts while either object is too "distorted" for a straightforward perturbative approach to be applicable. As mentioned above, a black hole settles into a stationary state very rapidly, and hence from a computational perspective there is little to gain in switching to a perturbative treatment to measure the ringdown waves. By contrast, in certain ranges of parameter space a hypermassive neutron star can last for several seconds before collapsing to a black hole, which for the full coupled Einstein-matter equations would be too expensive to evolve at present [a rough estimate of the cost is $O(1{,}000)$ CPU hours per millisecond at "modest" resolution].

3.1. Properties of Gravitational Wave Emission

During the early inspiral stage, in which velocities are much smaller than c, to leading order the emission of gravitational waves is proportional to the acceleration of the reduced (trace free) quadrupole moment tensor $Q_{ij}(t)$ of the system (this is textbook material, though for a couple of recent review articles see Flanagan & Hughes 2005, Buonanno 2007):

$$h_{ij}^{\rm TT}(t,\vec{x}) = \frac{2G}{rc^4}\frac{\partial^2 Q_{kl}(t-r)}{\partial t^2}\left[\perp_i^k \perp_j^l - \frac{1}{2}\perp^{kl}\perp_{ij}\right] \tag{1}$$

In the above, $h_{ij}^{\rm TT}$ is the perturbation of the spatial components of the Minkowski metric η_{ij} in the transverse traceless (TT) gauge, written in a Cartesian coordinate system $(t,\vec{x}) = (t, x_i)$. In this gauge there are no space-time or time-time perturbations of $\eta_{\mu\nu}$; i.e., $h_{tt}^{\rm TT} = h_{tj}^{\rm TT} = 0$. The center of mass of the source is at the origin, and the above expression assumes the perturbation is measured at a distance $r = |\vec{x}|$ much greater than the characteristic size of the source, here $\sim r_{\rm p}$, the periapse of the orbit. (We use the periapse here rather than, say, the semimajor axis, because for highly eccentric systems described later the dominant gravitational wave emission only occurs around periapse passage. Thus r_p more conveniently characterizes the relevant scale of gravitational wave emission for all eccentricities.) The projection tensor $\perp_{ij} = \delta_{ij} - \hat{n}_i\hat{n}_j$, with $\hat{n}_i = x_i/r$, i.e., $\hat{n}_i$, is the unit spatial vector from the source to the observer at location x_i. The above expression is (to leading order) valid in an expanding Universe if the distance r is replaced by the luminosity distance D_l and time is dilated by a factor $1+z$, where z is the redshift between the source and the observer.

The projection in Equation 1 encodes the property from general relativity that there are only two linearly independent propagating degrees of freedom, called the cross and plus polarizations. Thus the tensor $h_{ij}^{\rm TT}$ only has two independent nonzero components, which are called h_+ and $h_{\rm x}$. To illustrate, ignoring back reaction, a binary on a circular Keplerian orbit with orbital frequency $\omega = \sqrt{2GM/r_p^3}$ produces a radiation pattern

$$h_+(t,r,\theta,\phi) = \frac{4G}{rc^4}\mathcal{M}^{5/3}(2\omega)^{2/3}\cos(2\omega t+\phi)\left[\frac{1+\cos^2\theta}{2}\right], \tag{2}$$

$$h_{\rm x}(t,r,\theta,\phi) = \frac{4G}{rc^4}\mathcal{M}^{5/3}(2\omega)^{2/3}\sin(2\omega t+\phi)\cos(\theta); \tag{3}$$

here the so-called chirp mass $\mathcal{M} = \eta^{3/5} M$, the symmetric mass ratio $\eta = m_1 m_2 / M^2$, θ is the angle between the observer's line of sight and the axis normal to the plane of the binary, and ϕ is the (arbitrary) initial azimuthal phase.

The above expressions highlight several properties about gravitational emission from compact objects relevant for detection. First, gravitational wave detectors are directly sensitive to the amplitude of the metric perturbation and not the energy it carries. The former decays as $1/r$, whereas the latter decays as $1/r^2$ (and being proportional to the square of the third time derivative of Q_{ij}); hence an n-fold improvement in the sensitivity of detectors results in an n^3 increase in the observable volume of the Universe. The "advanced" upgrades to the first generation of ground-based interferometric detectors (that will be completed near the end of the decade) are expected to achieve an order-of-magnitude increase in sensitivity over initial LIGO readings, increasing the range over which binary neutron stars could be observed to hundreds of megaparsecs and binary black holes to billions of parsecs (Abadie et al. 2010). Note, however, that these distances assume matched filtering is used to search for signals that would otherwise be buried in detector noise. For this to maximize both detection prospects and parameter extraction requires template waveforms that are phase-accurate to within a fraction of a cycle over the most sensitive band of the detectors [which for Advanced LIGO (adLIGO) ranges from ~10 Hz to ~1 kHz]. Over the past two decades this has been the primary goal of the source modeling community; it is being achieved using high-order perturbative methods for the early inspiral, numerical solution for late inspiral and early merger, and perturbations off a single black hole afterward.

Second, the emission is clearly not isotropic. Only plus-polarized waves are radiated along the equator, and the amplitude is half of that radiated along the pole orthogonal to the orbit. Thus the distance to which a source can be observed strongly depends on its relative orientation to the detector. Importantly, however, this radiation is not strongly beamed, and so even nonideal orientations of the source to the detector can yield detectable signals.

Third, though these expressions only hint at a couple, there are several degeneracies in the signal that could limit accurate extraction of all relevant parameters from a detection. Under radiation reaction the orbit shrinks, and a binary will sweep across a range of frequencies ω, terminating at merger where $\omega_m \approx c^3 / GM$. If ω_m is not in band (such as with a binary neutron star merger), at leading order there is essentially complete degeneracy between the chirp mass and the distance to the source. If an electromagnetic counterpart could be observed and a redshift determined, the degeneracy would break. Higher-order effects, in particular if the black holes spin or the masses are unequal, excite higher gravitational wave multipoles that can further lift degeneracies. This demonstrates the need to understand the full details of the gravitational wave emission and, if matter is involved, possible electromagnetic counterparts. And as is discussed more throughout this review, such multimessenger observations could bring us a wealth of information beyond just measuring binary parameters.

3.2. Priors on Binary Parameters

Merger simulations are computationally expensive, taking of order 10^4–10^5 CPU hours for a simulation of the last $O(10)$ orbits of a quasi-circular inspiral of a binary black hole system. This may not sound too extreme, though remember this is just a single point in an eight-dimensional parameter space—mass ratio, six components of the two spin vectors, and eccentricity. The cost goes up with nonvacuum binaries for several reasons. First, in addition to gravity the relevant matter equations (relativistic hydrodynamics at least) need to be solved for. Second, the effective parameter space grows larger. This is in part to characterize unknown physics such as the equation of state (EOS) of matter at nuclear densities and in part because of new initial conditions, for example,

a neutron star's magnetic field configuration. Third, computational fluid dynamics algorithms are typically lower order (to be able to deal with shocks and surfaces) than the high-order finite difference or pseudospectral methods used to solve the Einstein equations, hence higher resolution is required for similar accuracy to a comparable vacuum merger.

The preceding discussion highlights that compact object merger simulations are too demanding to perform a naive, uniform sampling of parameter space to guide the construction of gravitational wave template banks. A promising approach to achieve a more optimal sampling uses the reduced basis method (Field et al. 2011), though regardless of the method one can ask, What priors can be placed on the range of parameters from either theoretical or observational considerations?

A typical neutron star likely has a mass within the range of $\approx$1 to 2.5 $M_\odot$ and a radius (which for a given mass is determined by the EOS) in the range of $\approx$8 to 15 km, and they are thought to have low spins (see, e.g., Lattimer & Prakash 2010). For black holes, an obvious theoretical restriction on the spin magnitude is that $|a| \leq 1$. Observations of candidate black holes, assuming general relativity is correct and black holes satisfy the bound, are beginning to provide estimates of spins ranging across all possible magnitudes $|a| \in [0, 1]$ (McClintock et al. 2011; McClintock, Narayan & Steiner 2013). The framework of classical general relativity does not provide predictable power when naked singularities arise, and without any theoretical/observational guidance perhaps the best one can do with gravitational waves is to seek for inconsistencies from the predictions of general relativity using something akin to the parameterized post-Einsteinian approach (Yunes & Pretorius 2009). [For tests of gravity with electromagnetic signals see, e.g., Broderick et al. (2014).] Theoretical models suggest the relative orientation of spins are not uniform, due either to properties of the progenitor binary for stellar mass systems or to interactions with surrounding matter or spin-orbit resonant effects during inspiral (Bogdanovic, Reynolds & Miller 2007; Gerosa et al. 2013). Nevertheless, neither theory nor observation provides a sufficiently compelling case to dismiss the full range of spins allowed by general relativity. For stellar mass black holes, masses are expected to range from a few to possibly hundreds of solar masses; supermassive black holes lie at least within the range 10^6–10^{10} $M_\odot$, and evidence is mounting for intermediate-mass black holes between this range (see, e.g., Greene & Ho 2004; Farrell et al. 2009; Godet et al. 2009; Shankar 2009; Davis et al. 2011; Kamizasa, Terashima & Awaki 2012; Casares & Jonker 2014). Consequently, these ranges are sufficiently broad that the mass ratio q is essentially unconstrained, in particular for the closer-to-comparable mass binaries that would require full numerical solution.

One parameter has been argued as being constrainable, especially for stellar mass binaries: the orbital eccentricity. The reason for this is that the back reaction of gravitational wave emission on the orbit tends to reduce eccentricity. To leading order under radiation reaction, the following is a decent approximation to the relationship between periapse and eccentricity [see Peters (1964) and Peters & Mathews (1963) for the derivation and full expression]:

$$r_{\rm p} \approx r_{\rm p0} \frac{1+e_0}{1+e} \left(\frac{e}{e_0}\right)^{12/19}, \tag{4}$$

where $r_{\rm p0}$, e_0 are the initial periapse and eccentricity, respectively. For the moderate initial eccentricities expected when the progenitor of the black hole binary is a stellar binary, $e \sim (r_{\rm p}/r_{\rm p0})^{19/12}$. Such a binary enters the adLIGO band at $r_p \sim 10^2$ km, whereas expected values for $r_{\rm p0}$ are several orders of magnitude larger (see, e.g., Kalogera et al. 2007), hence e will be completely negligible here. This has focused the majority of work on mergers on the quasi-circular $e = 0$ case. However, there are other mechanisms to form binaries, and some could lead to systems that have high eccentricity while emitting in the LIGO band. These mechanisms include dynamical capture from gravitational wave emission during a close two-body encounter in a dense cluster (O'Leary, Kocsis & Loeb 2009; Lee, Ramirez-Ruiz & Van de Ven 2010), a merger induced during a binary–single

star interaction in a similar environment (Samsing, MacLeod & Ramirez-Ruiz 2014), and Kozai-resonant enhancement of eccentricity in a hierarchical triple system (Wen 2003; Kushnir et al. 2013; Seto 2013; Antognini et al. 2014; Antonini, Murray & Mikkola 2014). Event rates are highly uncertain for both classes of binaries [see Abadie et al. (2010) for a review of quasi-circular inspiral systems, and East et al. (2013), Kocsis & Levin (2012), Lee, Ramirez-Ruiz & Van de Ven (2010), O'Leary, Kocsis & Loeb (2009), and Tsang (2013) for discussions of dynamical capture systems], and though quasi-circular inspirals are likely dominant, eccentric mergers may not be completely irrelevant as often assumed in the gravitational wave community. The formation mechanism for supermassive black hole binaries is different (being driven by mergers of the host galaxies of individual black holes), though similarly there are arguments that in some cases non-negligible eccentricity might remain until merger (Roedig & Sesana 2012).

The difficulty with eccentricity is that it is not "merely" an additional parameter but changes the qualitative properties of a merger in a manner that challenges both source modeling and data analysis strategies. With regard to modeling, the orbital period increases significantly with e for a given r_p, making numerical simulations of multiorbit mergers very expensive. Perturbative methods have not yet been developed to high order for large eccentricity orbits (though see Bini & Damour 2012). Taken together it may be unreasonable to expect templates accurate enough for data analysis using matched filtering any time soon, and different (though suboptimal) strategies may need to be developed, for example, power stacking (East et al. 2013). This implies that for practical purposes there are two "classes" of binaries—quasi-circular inspirals and large eccentricity, small initial pericenter mergers.

Having discussed broad considerations relevant to the three classes of binaries (black hole–black hole, black hole–neutron star, neutron star–neutron star), we now discuss salient features of each class uncovered through numerical simulations.

4. BINARY BLACK HOLES

Due to the "no-hair" property of event horizons in four-dimensional Einstein gravity, isolated single black holes in our Universe are expected to be described almost exactly by the Kerr family of solutions. This is a two-parameter family, labeled by the total gravitational mass M and angular momentum J. (An isolated black hole can also have a conserved charge, though in astrophysical settings black holes should be uncharged to excellent approximation. "Exotic" matter fields could also support additional "hair," though we do not consider such fields here.) The latter is more conveniently described by a dimensionless spin parameter, $a = J/M^2$. As mentioned, an event horizon is only present if $|a| \leq 1$, otherwise the solution exhibits a naked singularity. If such a situation could arise (violating the so-called cosmic censorship conjecture), classical general relativity would describe neither the exterior solution nor the dynamics of the object in our Universe. This would offer a prime opportunity to study quantum gravity, though unfortunately to date no theoretical studies of plausible astrophysical processes involving dynamical, strong-field gravity, including gravitational collapse and compact object mergers, have found a naked singularity arising dynamically. [Though see Jacobson & Sotiriou (2009) for an intriguing suggestion that near extremal black holes could be "over spun" and Shapiro & Teukolsky (1991), who suggest that collapse of matter with negligible self-pressure and in a highly prolate configuration could lead to naked singularities. It is also well known that naked singularities can arise in spherical collapse of ideal fluids (see, e.g., Joshi 2013) or critical collapse in a larger class of matter models (see, e.g., Gundlach 2003). However, these examples are either nongeneric (whether by imposed symmetries or fine tuning of initial data) or arise in matter that is of arguable relevance to collapse in astrophysical settings (Wald 1997).]

Thus, technical details aside, the study of vacuum binary black hole mergers in general relativity is a well-defined problem characterized by a relatively small set of parameters: the mass ratio q of the binary, the two initial spin vectors $\vec{s}_1, \vec{s}_2$ of each black hole, the initial eccentricity e_0, and the size of the orbit (parameterized, for example, by the initial pericenter distance $r_{\rm p0}$). There is no intrinsic scale in vacuum Einstein gravity, hence there is a trivial map from any solution with a given set of these parameters to a desired total mass M of the binary. In the remainder of this section we present results from the numerical solution of the Einstein field equations for vacuum mergers, discuss some astrophysical consequences, and briefly comment on issues related to testing general relativity from gravitational wave observations of vacuum mergers. For other review articles discussing similar topics see Centrella et al. (2010), Hannam (2013), and Pretorius (2009).

4.1. Results and Applications of Merger Simulations

A couple of important qualitative questions about the merger process have largely been answered. The first relates to cosmic censorship: A broad swath of parameter space has been explored (see, for example, Hinder et al. 2013), and no naked singularities have been found. Furthermore, to the level of scrutiny the solutions have been subjected, the late time behavior is consistent with a spacetime approaching a Kerr solution via quasi-normal mode decay. (In theory the quasi-normal ringdown should transition to a power-law decay at very late times. This has been verified for perturbed single black holes. Binary simulations have not yet been carried that far beyond merger, though the motivation for doing so is minimal as the amplitude of these power-law tails is too small to be observable.) The second relates to the existence of new "phases" of the merger outside the purview of the perturbative treatments governing the inspiral and ringdown. One line of reasoning argues that owing to the nonlinearity of the field equations and the fact that the late stages of a merger occur in the most dynamical, strong-field regime of the theory, these phases would be natural places to expect novel physics. The opposing argument, which turned out to better describe the simulation results, is that the merger is effectively a highly dissipative process that occurs deep within the gravitational potential well of the combined objects, and very little of the spacetime dynamics that occurs there will leave an imprint on the waves radiated outward. Or stated another way, perturbative methods have been extended to quite high order in v/c in both the conservative and dissipative dynamics of a binary, and black hole perturbation theory begins with an exact strong-field solution; these together capture the "essential" nonlinearities of the problem. As a consequence of this rather smooth behavior a convenient approach to constructing templates is the effective one-body (EOB) method (Buonanno & Damour 1999), where resummed PN inspiral waveforms are smoothly attached to quasi-normal ringdown modes via a transition function calibrated by numerical simulations (for some recent papers, see Ajith et al. 2011; Damour, Nagar & Bernuzzi 2013; Pan et al. 2014). Most of the work in this regard has been conducted on nonprecessing orbits (i.e., any net spin angular momentum is aligned with the orbital angular momentum) or lower-spin black holes, and it remains to be seen how well this technique may work for highly spinning black holes in precessing orbits. See **Figure 1** for two examples of gravitational wave emission from merger simulations and, for one of them, a match to EOB calculations.

The science gleaned from numerical simulations of vacuum binary mergers has therefore mostly been in details of the process. Important numbers of relevance to astrophysics include the total energy and angular momentum radiated during merger (and consequently the final mass and spin of the remnant black hole) and the recoil or "kick" velocity of the final black hole to balance net linear momentum radiated. We cannot possibly list these numbers for all cases simulated to date (but we do give some citations to relevant literature for further information). To give a sense of

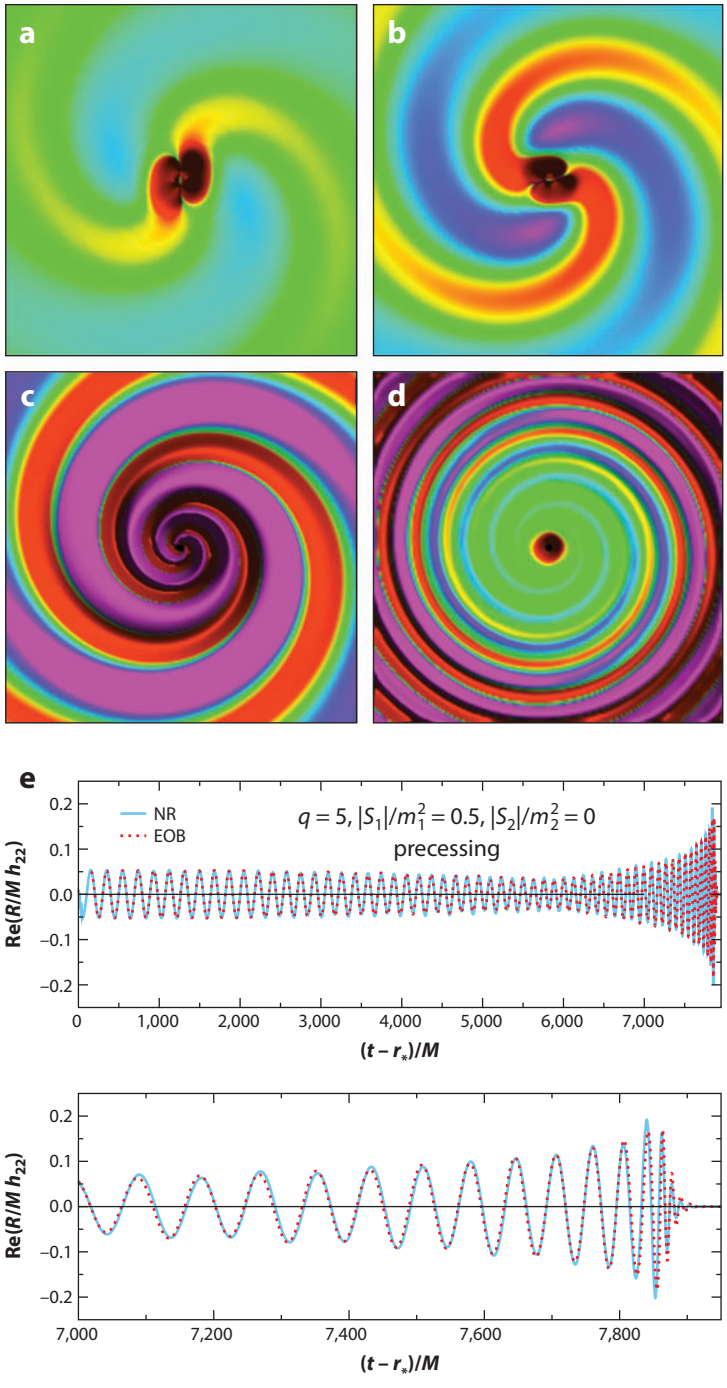
a
b
c
d
e
NR
EOB
$q = 5, |S_1|/m_1^2 = 0.5, |S_2|/m_2^2 = 0$
precessing
$\mathrm{Re}(R/M\, h_{22})$
$(t - r_*)/M$
0.2
0.1
0.0
−0.1
−0.2
0
1,000
2,000
3,000
4,000
5,000
6,000
7,000
7,200
7,400
7,600
7,800

the physics and order of magnitude of the numbers, we highlight a few key results and present some of the simpler fitting formulas.

4.1.1. Energy radiated. One can think of the energy radiated during a merger as coming from two sources: the gravitational binding energy liberated during inspiral and energy in the geometry of the merger remnant formed during the collision that is emitted as the horizon settles down to its stationary Kerr state (on timescales comparable with the final orbital period). In the extreme-mass-ratio limit the former dominates, and the total radiated energy equals the magnitude of the binding energy at the ISCO; for a quasi-circular inspiral this ranges from ∼3.8–42% of the rest mass of the small black hole, depending on the spin of the large black hole; the lower (upper) limit is a retrograde (prograde) equatorial orbit about an extremal Kerr black hole (the Schwarzschild case gives 5.7%). As the mass ratio decreases (i.e., the masses become comparable), the emitted energy increases, and the amount coming from the ringdown grows to a comparable fraction approaching the equal mass limit. Here numerical simulations are required to compute the exact numbers, and it is more useful to quote the value as a percentage of the total gravitational energy M (the gravitational mass of the system as measured by an asymptotic observer). A useful formula interpolating between the analytic extreme-mass-ratio limit (Equation 5, *top line*) and empirical fits to numerical data (Equation 5, *bottom line*) was derived by Barausse, Morozova & Rezzolla (2012; see Lousto et al. 2010 and Tichy & Marronetti 2008 for a couple of alternative formulas):

$$\frac{E_{\rm rad}}{M} \approx \eta(1-4\eta)[1-\tilde{E}_{\rm ISCO}(\tilde{a})] + 16\eta^2[p_0 + 4p_1\tilde{a}(\tilde{a}+1)]. \quad (5)$$

Here $\tilde{a} = \vec{L}\cdot(\vec{S}_1+\vec{S}_2)/M^2$ is the projection of the sum of the black hole spin vectors onto the orbital angular momentum prior to merger, $p_0 \approx 0.048$, $p_1 \approx 0.017$; and $\tilde{E}_{\rm ISCO}(\tilde{a})$ is the energy of the effective ISCO of the system. This formula fits existing numerical simulation results to within better than a percent in most cases (see Barausse, Morozova & Rezzolla 2012 for comparisons and more details).

4.1.2. Final spin. There are numerous formulas characterizing the final spin of the merger remnant that have been constructed via fits to NR results [e.g., Barausse & Rezzolla (2009) and Tichy & Marronetti (2008); see also Lousto et al. (2010) for PN-inspired functions and Boyle, Kesden & Nissanke (2008) for a prescription based on a so-called spin expansion that uses symmetry arguments to economize the formulas). Here we give a simple first-principles-derived expression from

Figure 1

(*a*) A depiction of the gravitational waves emitted during the merger of two equal-mass (approximately) nonspinning black holes. Reprinted from Buonanno, Cook & Pretorius (2007) with permission. Shown is a color map of the real component of the Newman-Penrose scalar Ψ_4 multiplied by r along a slice through the orbital plane, which far from the black holes is proportional to the second time derivative of the plus polarization (*green* is 0, toward *violet* is positive, and toward *red* is negative). (*a*,*b*) The dominantly quadrupolar inspiral waves ∼150 M and ∼75 M before merger, respectively. (*c*) Near the peak of the wave emission at merger, and (*d*) the ringdown waves propagating out ∼75 M after merger. The size of each box is around $(100\ M)^2$. (*e*) Gravitational wave emission measured from a numerical relativity simulation of a binary black hole merger (NR) overlaid with an NR-calibrated effective one-body (EOB) calculation. Reprinted from Taracchini et al. (2014) with permission. The binary has a mass ratio $q = 5$, the more massive black hole has a dimensionless spin of $a = 0.5$ with direction of the spin axis initially in the plane of the orbit, and the second less-massive black hole is nonrotating. That the amplitude of the wave is not monotonically increasing during inspiral is a manifestation of the modulation induced by precession of the orbital plane.

Buonanno, Kidder & Lehner (2008) that captures the basic physics and agrees reasonably well with numerical results. The following formula is valid for spins aligned with the orbital angular momentum (see Kesden, Lockhart & Phinney 2010 and others cited above for generalizations to precessing binaries):

$$a_f M \approx L_{\rm orb}(r_{\rm ISCO}, a_f) + m_1 a_1 + m_2 a_2. \quad (6)$$

Here $a_f M$ is the spin angular momentum of the remnant (with M approximated by $m_1 + m_2$), $m_1 a_1$ and $m_2 a_2$ are the spin angular momenta of the initial black holes, and $L_{\rm orb}(r_{\rm ISCO}, a_f)$ is the orbital angular momentum of a reduced-mass particle equivalent of the system evaluated at the ISCO of a Kerr black hole using the parameters of the remnant. The interpretation of this is straightforward: The system radiates angular momentum until the plunge to merger, after which the majority of the remaining spin plus orbital angular momentum is subsumed by the final black hole. Some angular momentum is radiated during ringdown, but this is taken into account in the above formula through the use of the effective ISCO of the remnant black hole. For interest, a quasi-normal mode with frequency ω_m and azimuthal multiple number m has the following relationship between the energy and angular momentum it carries: $J_{\rm rad} \approx (m/\omega_m) E_{\rm rad}$. $m = 2$ is the dominant mode, and for example a Schwarzschild black hole has $\omega_2 \approx 0.38/M$ (Berti, Cardoso & Starinets 2009). Though it is not possible to clearly differentiate the quasi-normal part of the wave from the emission that precedes it, a rough estimate is that of order 1–2% of the net energy is emitted in the ringdown for comparable mass mergers.

Equation 6 predicts the final spin to within a few percent in many cases. For example, it gives $a_f/M \approx 0.663$ for the merging of equal mass, nonspinning black holes; comparing with NR simulations, an initial estimate was $a_f/M \approx 0.70$ (Pretorius 2005); the latest high-accuracy simulations refine it to $a_f/M \approx 0.6865$ (Scheel et al. 2009).

4.1.3. Recoil. A recoil in the remnant, namely a velocity postmerger relative to the initial binary center of mass, can arise when there is asymmetric beaming of radiation during the merger. Asymmetry comes from unequal masses and black hole spins. The formulas describing the recoil can be rather involved (see, for example, Lousto & Zlochower 2011), so here we briefly mention some of the salient features and numbers. Nonspinning binaries with mass ratio q different from unity give rise to a recoil in the plane of the binary, reaching a maximum of $\sim$175 km s^{-1} (Baker et al. 2006, Berti et al. 2007, González et al. 2007, Herrmann et al. 2007) for $q \approx 1/3$. Spin introduces additional asymmetry in the radiation by causing the orbital plane to precess and "bob," which can induce a recoil both in and orthogonal to the plane of the binary. The magnitude of the out-of-plane recoil is sinusoidally modulated by the effectively random initial phase of the binary. Spin can also allow the onset of a plunge to occur at higher frequency and, hence, give higher gravitational wave luminosity, which further amplifies the recoil. The bobbing motion (see Pretorius 2009 for an intuitive description) is associated with the largest recoils, which remarkably can reach several thousand kilometers per second for appropriately aligned high-magnitude spins (Campanelli et al. 2007, González et al. 2007, Lousto & Zlochower 2011); see **Figure 2*a*** for examples.

These largest velocities are well in excess of the escape velocities of even the most massive galaxies. That observational evidence suggests most galaxies harbor central supermassive black holes, together with hierarchical structure formation models of the growth of these galaxies, implies that mergers with very large recoils are rare. If mergers themselves are common, and black holes can have sizable spins as implied by current observations (Reynolds 2013), then the typical recoil must be significantly less than the maximum theoretically possible. One possible explanation for this would be if most mergers take place in gas-rich environments, because then torques induced by circumbinary material will tend to align the spins of the black holes with the

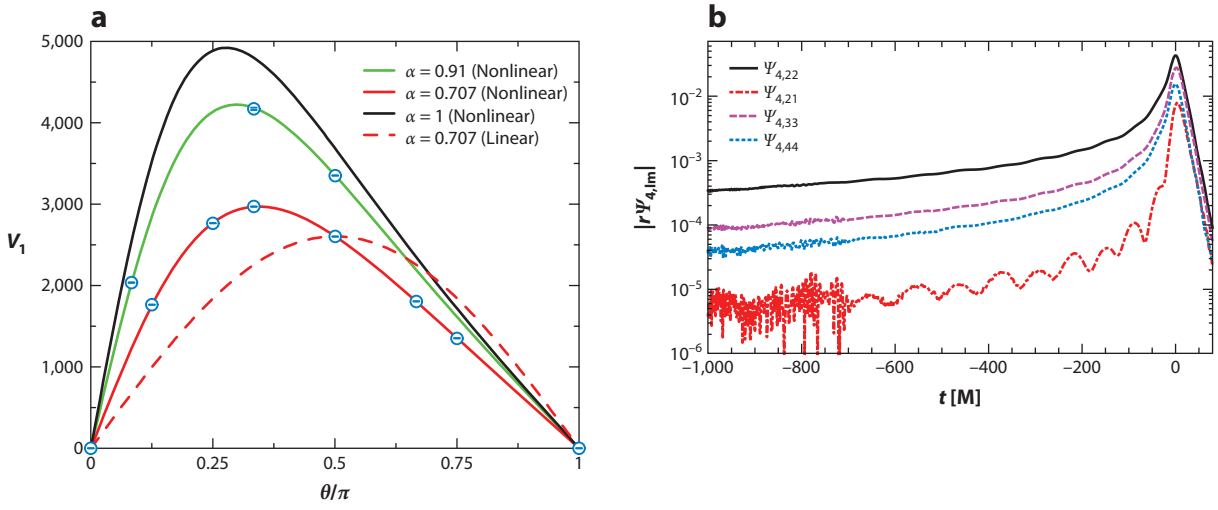

Figure 2

(*a*) Recoil velocities from equal-mass, spinning binary black hole merger simulations (*circles*) together with analytical fitting functions. Each black hole has the same spin magnitude α, equal but opposite components of the spin vector within the orbital plane; θ is the initial angle between each spin vector and the orbital angular momentum. The dashed line corresponds to a fitting formula that depends linearly on the spins, whereas solid lines add nonlinear spin contributions. Reprinted from Lousto & Zlochower 2011 with permission. (*b*) Strength of different modes in the gravitational waves from a binary black hole merger with mass ratio $M_1/M_2 = 3$, and spins $a_1 = 0.75$, $a_2 = 0$. This system exhibits a marked precession that complicates the multipolar mode structure seen in a fixed observer's frame. However, a transformation to a coprecessing "quadrupole aligned" frame, as shown in this figure, illustrates that the main radiation channel is still the $l = 2, m = 2$ mode. Reprinted from Schmidt et al. (2011).

overall orbital angular momentum, a configuration that has significantly lower maximum recoil (see, e.g., Bogdanovic, Reynolds & Miller 2007; Dotti et al. 2010). Another possible explanation that operates even in vacuum comes from PN calculations that include spin-orbit coupling, which shows a tendency for the black hole spins to align (antialign) with each other if the spin of the more massive black hole is initially at least partially aligned (antialigned) with the orbital angular momentum (Kesden, Sperhake & Berti 2010).

4.1.4. Tests of general relativity. A further opportunity offered by gravitational wave observations of merging binaries is to test dynamical, strong-field gravity. With obvious caveats associated with our present lack of understanding of dark matter and dark energy, general relativity has so far been shown to provide a consistent description of gravity in all observations and experiments that are constrained by its predictions (see, e.g., Will 2006). Lacking here are tests in the most nonlinear regime of the theory, in particular where black holes can form. Certainly there is no doubt about the existence of massive, dark, ultracompact objects, and observations of (for example) X-ray emission from stellar mass candidates or properties of AGNs are consistent with these phenomena being powered by Kerr black holes. However, that horizon scales cannot be quite resolved at present [this may change within a few years through VLBA observations of our Galaxy's central black hole, SGA* (Broderick, Loeb & Narayan 2009; Broderick et al. 2011) as well as nearby M87 (Doeleman et al. 2012)], together with complexities of the matter physics responsible for the emission, prevents precise determination of local properties of the spacetime. Binary black hole mergers, in particular stellar mass systems that are expected to occur largely in vacuum, offer a unique opportunity to study pure, strong-field gravity. General relativity's

ability to predict the entire waveform, which is uniquely determined by a small set of numbers ($M, q, e, \vec{s}_1, \vec{s}_2$, and detector-source orientation parameters) and can consist of hundreds or even thousands of cycles in the LIGO band, can in principle allow for stringent self-consistency tests on high signal-to-noise–ratio (SNR) events.

However, there are several issues that complicate general relativity's promise in testing in the near future. First, given the lack of events from the initial LIGO observing runs, it is unlikely that adLIGO will observe a very loud event. Hence viable tests may require statistical analysis of a number of low-SNR events, and little work has yet been done to suggest how this might be carried out [see Agathos et al. (2014) for a recent proposal; related work on constraining the nuclear EOS using multiple mergers events involving neutron stars is also beginning to be investigated—see the discussion in Section 5]. Second, detection and parameter estimation relies on matched filtering with templates. If the only templates used are those constructed using general relativity, then all information about possible deviations will be projected out. (Note also that it is unlikely that general relativity templates will completely "miss" all events even if there are strong-field deviations. This is because binary pulsar observations confirm the leading order radiative dynamics of general relativity.) If the event has a high SNR, there should be a detectable residual excess power, but again for the typical SNRs expected for adLIGO this is unlikely. [This is not the case for possible space-based detectors, like eLISA and its exquisite SNR, which allows for detecting supermassive binary black holes mergers with masses in the range $10^4 M_\odot < M < 10^7 M_\odot$ out to redshifts of $z \simeq 20$ with a SNR ≥ 10. For a recent review see Seoane et al. (2013).] Compounding the problem, despite the large number of proposed alternatives or modifications to general relativity (see, for example, Will 1993, 2006), almost none have yet been presented that (*a*) are consistent with general relativity in the regimes where it is well tested, (*b*) predict observable deviations in the dynamical strong field relevant to vacuum mergers, and (*c*) possess a classically well-posed initial value problem to be amenable to numerical solution in the strong field. The notable exceptions are a subset of scalar tensor theories, though these require a time-varying cosmological scalar field for binary black hole systems (Horbatsch & Burgess 2012) or one or more neutron stars in the merger (see Section 5). Thus there is little guidance on what reasonable strong-field deviations one might expect. Proposed solutions to (at least partially) circumvent these problems include the parameterized post-Einsteinian and related frameworks (Yunes & Pretorius 2009, Agathos et al. 2014) and modified PN waveforms (Arun et al. 2006), as well as exploiting properties of the uniqueness of Kerr and its quasi-normal mode structure (Collins & Hughes 2004; Berti, Cardoso & Will 2006).

4.1.5. Eccentric binaries. As mentioned above, the majority of the work on binary black hole mergers from the relativity community has focused on quasi-circular inspiral, except for a handful of recent studies (Pretorius & Khurana 2007; Healy, Levin & Shoemaker 2009; Gold & Bruegmann 2013). One of the interesting results is that so-called zoom-whirl orbital dynamics is possible for comparable-mass binaries. In the test particle limit, zoom-whirl orbits are perturbations of the class of unstable circular geodesics that exist within the ISCO. They exhibit extreme sensitivity to initial conditions, in which sufficiently fine-tuned data can give an arbitrary number of near-circular "whirls" at periapse for a fixed eccentricity. Away from the test particle limit, gravitational wave emission adds dissipation to the system; however, what the simulations show is that even in the comparable mass limit the dissipation is not strong enough to eradicate zoom-whirl dynamics, but merely limits how long it can persist. Perhaps the most interesting consequences of high-eccentricity mergers could arise when neutron stars are involved; this is discussed in Section 5.

For the vacuum problem, aside from providing information on binary formation channels, high-eccentricity events could in principle offer the most stringent tests of strong-field gravity.

The reason is due to the nature of these orbits compared with quasi-circular inspiral: Significantly higher velocities are reached at periapses passage, a larger fraction of the total power is radiated in this high v/c regime, and the long time between periapse bursts imply that small deviations in emission could result in large dephasing of the waveform from one burst to the next. However, to date no studies have addressed in any quantitative manner how well general relativity can be constrained using eccentric mergers.

4.2. Further Physics

With the vacuum merger problem essentially under control, the field is now more closely examining the impact a merging black hole binary can have on its astrophysical environment. The most pertinent scenario is a supermassive binary merger, and questions relate to how the rapidly changing gravitational field, ensuing gravitational waves, and possible recoil could perturb surrounding gas, plasma, electromagnetic fields, stars, etc. Here we briefly discuss some of the more interesting and potentially observable phenomena revealed by recent studies.

4.2.1. Prompt counterparts to supermassive binary black hole mergers within circumbinary disks. First studies of the interaction of binary black holes with surrounding electromagnetic fields and plasma were presented by Palenzuela et al. (2010) and Palenzuela, Lehner & Leibling (2010). Though not modeled there, the expected source of these fields and plasma would be a circumbinary disk. More recent work has begun to self-consistently model the disk as well (Farris et al. 2012, Gold et al. 2014). Recall that in the case of a single black hole, the Blandford-Znajek (BZ) mechanism (Blandford & Znajek 1977) indicates the plasma (coming from an accretion disk) is able to tap rotational energy from the black hole and power an energetic Poynting flux. Tantalizing observational evidence linking the strength of radio signals and black hole spin has been presented by McClintock, Narayan & Steiner (2013). In the context of binary black holes, simulations demonstrated that the spacetime helps stir electromagnetic field lines and that, akin to the BZ mechanism, the plasma is able to tap translational and rotational energy from the system to produce dual jets (Palenzuela et al. 2010; Palenzuela, Lehner & Leibling 2010; see also **Figure 3**). These jets would act as spacetime tracers, and their behavior can be modeled reasonably well by an extension of the BZ formula. That is, prior to merger, the luminosity from the system obeys $L \simeq B^2 \sum_{i=1,2} [\Omega_{\rm H}(i)^2 + \kappa v(i)^2]$, where $\Omega_{\rm H}(i)$, $v(i)$, and κ are the angular rotational velocities of the horizons, the black hole velocities, and a relative strength parameter, respectively. [The dependence on $\Omega_{\rm H}$ acquires higher-order corrections close to maximally spinning cases (Tchekhovskoy, Narayan & McKinney 2010).] (The value of $\kappa \simeq 100$ and indicates that black holes must be moving at $\gtrsim 0.1c$ for a nontrivial contribution unless, of course, they are nonspinning.) Notice that unlike the original BZ effect, even if the black holes are nonspinning there could be a sizable luminosity due to the contribution from the translational kinetic energies of the black holes (which can reach ≈ 0.2–$0.3c$ near merger for quasi-circular inspiral). After merger, a single jet arises with luminosity $L \simeq B^2(\Omega_{\rm H_{final}} + \kappa v^2_{\rm recoil})$ (though the second term is subleading unless the final black hole has negligible spin, as $v_{\rm recoil}$ is at most $\approx 0.015c$). This behavior implies interesting possibilities for detection of gravitational and electromagnetic waves associated with a merger embedded in a circumbinary disk (see, e.g., Mösta et al. 2012, O'Shaughnessy et al. 2011).

4.2.2. Postmerger consequences of supermassive binary black hole mergers. The merger event can have several interesting consequences due to the large amounts of energy radiated and (for appropriate spins and mass ratios) the recoil of the final black hole; we briefly mention a few here. For recent reviews of this and other astrophysical consequences, see Komossa

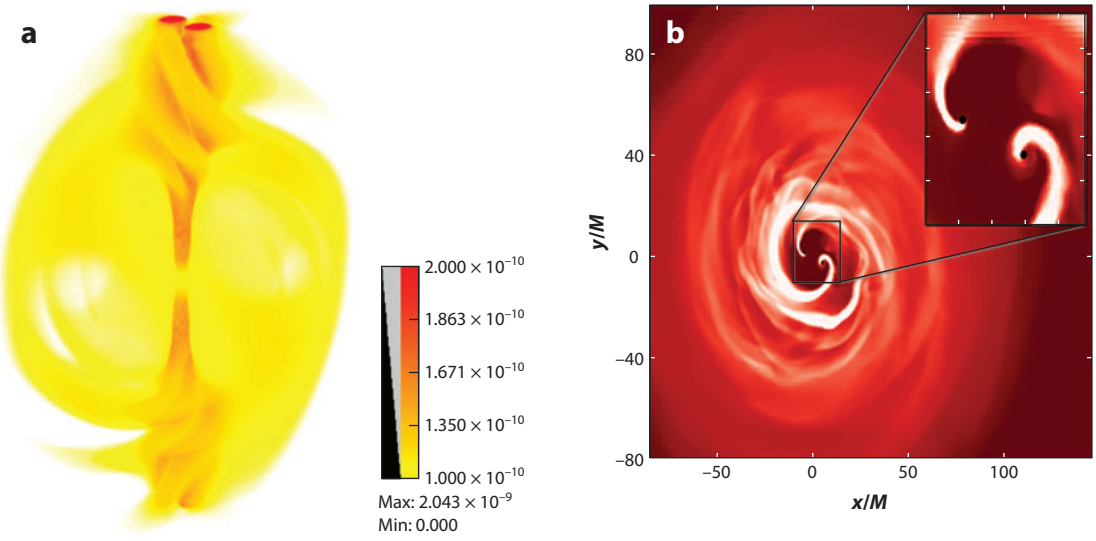

Figure 3

(*a*) Poynting flux produced by the interaction of an orbiting black hole binary with a surrounding magnetosphere. The "braided" jet structure is induced by the orbital motion of the black holes. Reprinted from Palenzuela, Lehner & Leibling (2010) with permission. (*b*) Rest-mass density induced by a supermassive black hole binary interacting with a magnetized disk prior to when the binary "decouples" from the disk, namely when the gravitational wave back reaction timescale becomes smaller than the viscous timescale. Reprinted from Farris et al. (2012) with permission.

(2012) and Schnittman (2013). With respect to timescales in the disk these effects occur essentially instantaneously. This near-impulsive perturbation of the gravitational potential in the outer parts of the accretion disk could lead to the formation of strong shocks, producing observable electromagnetic emission on timescales of a month to a year afterward (Lippai, Frei & Haiman 2008); subsequent inward migration of the disk could induce possible observable emissions (Milosavljević & Phinney 2005). The most favored orientations for recoils can produce velocities large enough to significantly displace the remnant from the galactic core or even eject the black hole from the host galaxy altogether (though as discussed above this is likely quite rare). If the system has a circumbinary accretion disk, the recoil would carry the inner part of the disk with it, and this could be observable in Doppler-displaced emission lines relative to the galactic rest frame (Komossa, Zhou & Lu 2008). Earlier studies have suggested that, prior to merging, the accretion rate, and hence the luminosity of the nucleus, would be low as the relatively slow migration of the inner edge of the accretion disk decouples from the rapidly shrinking orbit of the binary. Postmerger then, AGN-like emission could be reignited once the inner edge of the disk reaches the new ISCO of the remnant black hole. This should be displaced from the galactic center if a large recoil occurred and could be observable in nearby galaxies (see, for example, Loeb 2007). However, more recent simulations of circumbinary disks using ideal magnetohydrodynamics for the matter shows that complete decoupling does not occur, and relatively high accretion rates can be maintained all the way to merger (Bode et al. 2012, Farris et al. 2012, Noble et al. 2012) and afterward (e.g., Shapiro 2010). The binary orbit in this case causes a modulation in the luminosity of the system, which may be observable. A last effect we mention is that a displaced central black hole should also have its loss-cone refilled, increasing the frequency of close encounters with stars and their subsequent tidal disruption by the black hole, with rates as high as 0.1 year^{-1}; the disruption could produce observable electromagnetic emission (Stone & Loeb 2011).

4.2.3. Binary black hole mergers and galaxy formation. Galaxy formation models have also been exploited to understand the outcome of binary black hole mergers. There is strong stellar, gas-dynamical (Kormendy & Richstone 1995, Magorrian et al. 1998, Kormendy & Ho 2013), and electromagnetic (Gebhardt et al. 2000, Peterson et al. 2004) evidence for the existence of massive black holes at the centers of galaxies. These central black holes play a fundamental role in our current paradigm of galaxy formation and evolution; for example, they are required to explain quasar and AGN emission (Soltan 1982), as well as cosmic downsizing (Bower et al. 2006; Croton et al. 2006; Scannapieco, Silk & Bouwens 2005). In the ΛCDM model galaxies merge into increasingly larger ones as cosmic time proceeds, and consequently their massive black holes are expected to merge, initially via processes such as dynamical friction, with gravitational wave emission only taking over in the very late stages. Results from NR simulations have been utilized to follow the evolution of these black holes through coalescence. More specifically, a number of works studied the mass and spin evolution of supermassive black holes through cosmic time (Volonteri, Sikora & Lasota 2007; Berti & Volonteri 2008; Fanidakis et al. 2011; Volonteri et al. 2013), in some cases also accounting for the recoil velocity of the merger remnant (Barausse 2012, Lousto et al. 2012). It has also been suggested that if a space-based detector such as eLISA becomes available, measurements of the mass ratios of black hole binaries and the precession effects predicted by PN/NR calculations would help to discriminate between competing models of galaxy formation (Sesana et al. 2011, Barausse 2012).

5. NONVACUUM BINARIES

As in the binary black hole case, nonvacuum binaries present a well-defined problem; however they need a larger set of parameters to characterize. First, the matter physics introduces a scale, so that unlike the vacuum case the total mass of the system cannot be factored out. Thus the set of parameters needed to describe the orbit are now the masses m_1 and m_2 of the compact objects, their two initial spin vectors $\vec{s}_1, \vec{s}_2$ (which, however, are expected to be small for neutron stars), and the initial eccentricity e_0 and size of the orbit (again which we parameterized by the initial pericenter distance r_{p0}). Second, for neutron star matter one must specify the EOS (which for a given mass star determines its radius), and each star's magnetization (strength and dipole direction).

The presence of (magnetized) matter in the system, that is strongly affected by the rapidly varying geometry during coalescence, can naturally induce electromagnetic and neutrino emission in concert with the gravitational waves. A prime example is short gamma-ray bursts (sGRBs), and the evidence is mounting that nonvacuum binary mergers provide the central engine for these spectacular astrophysical phenomena (e.g., Janka et al. 1999; Lee & Ramirez-Ruiz 2007; Metzger & Berger 2012; Berger, Fong & Chornock 2013; Piran, Nakar & Rosswog 2013; Tanvir et al. 2013; Berger 2014). Thus, in addition to obtaining predictions for the gravitational wave signatures from these events (see **Figure 4** for some examples), research using simulations is also focused on gaining a theoretical understanding of their connections to sGRBs and related phenomena.

Widely separated nonvacuum binaries display the same behavior as binary black holes. Here internal details play a negligible role, as their effects first appear in a PN expansion at order $(v/c)^{10}$. Closer-to-merger tidal forces introduce subtle deviations at first, growing to quite large deformations at the point of contact in a binary neutron star system; for a black hole–neutron star system, such forces can even lead to the disruption of the star prior to merger. For binary neutron stars, if the total mass in the remnant is more than the maximum mass allowed by the EOS, a black hole will eventually form. The intermediate state is called a hypermassive neutron star (HMNS) and is temporarily supported by rotation and thermal pressure. An interesting question then, as illustrated in **Figure 4**, is, How long does the HMNS last? Once a black hole forms,

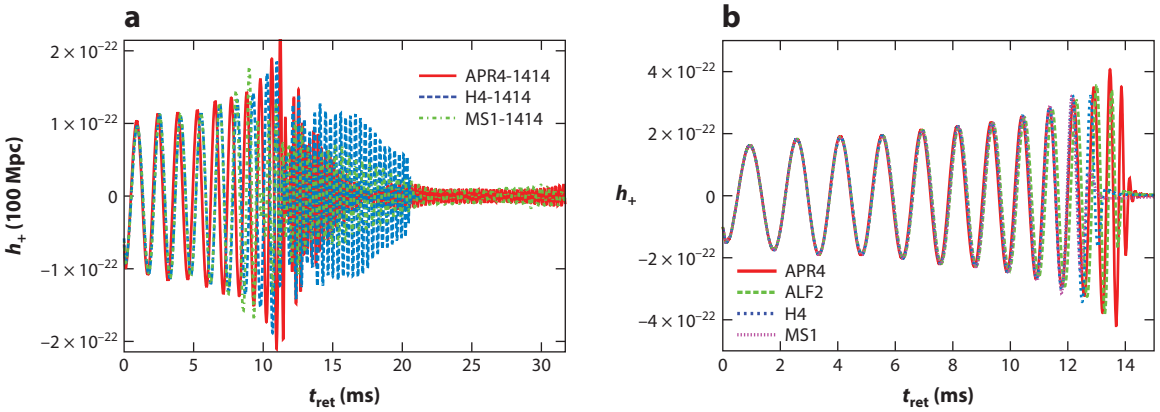

Figure 4

Examples of the "plus" polarization component of gravitational waves from binary neutron star mergers, measured 100 Mpc from the source along the direction of the orbital angular momentum. The different curves correspond to different choices of the equations of state (EOSs) of the neutron star matter, labeled APR4, ALF2, H4, and MS1. For a 1.4-$M_\odot$ neutron star, the APR4, ALF2, H4, and MS1 EOSs give radii of 11.1, 12.4, 13.6, and 14.4 km, respectively. (*a*) Mergers of an equal-mass binary neutron star system (with $m_1 = m_2 = 1.4\,M_\odot$). A hypermassive neutron star is formed at merger, but how long it survives before collapsing to a black hole strongly depends on the EOS. The H4 case collapses to a black hole ≈10 ms after merger; the APR4 and MS1 cases have not yet collapsed ≃35 ms after merger, when the simulations were stopped (the MS1 EOS allow a maximum total mass of $2.8\,M_\odot$, so this remnant may be stable). The striking difference in gravitational wave signatures is self-evident. Reprinted from Hotokezaka et al. (2013) with permission. (*b*) Emission from black hole–neutron star mergers, with $m_{BH} = 4.05\,M_\odot$, $m_{NS} = 1.35\,M_\odot$. Variation with EOSs is primarily due to coalescence taking place earlier for larger radii neutron stars (from Kyutoku, Ioka & Shibata 2013).

and following a black hole–neutron star merger, an accretion disk can form. If there is sufficient mass in the disk, this could be the beginning of a jet that would eventually produce a sGRB. A host of other electromagnetic emission is likely as a consequence of these nonvacuum mergers, as is neutrino emission. In the following sections, we discuss these in more detail, highlighting the information gained from NR simulations. For other review articles in this subject area, see Duez (2010) and Pfeiffer (2012).

5.1. Binary Neutron Star Mergers

Fully general relativistic studies of binary neutron stars have been an active area of research for over a decade. (For a small sample of recent results in this area see, e.g., Anderson et al. 2008b; Stephens, Shapiro & Liu 2008; Rezzolla et al. 2010; Sekiguchi et al. 2011; Kiuchi et al. 2012; Hotokezaka et al. 2013; Kaplan et al. 2014; Palenzuela et al. 2013a; Read et al. 2013). The initial focus of the research was directed toward understanding broad characteristics of the gravitational wave emission, and consequently rather simple treatments of the matter were employed (typically an ideal fluid with polytropic EOS). These efforts gave a rather robust understanding of the qualitative dynamics of the system and prepared a solid foundation to increase the realism of the matter modeling in the simulations. In recent years the addition of new physical ingredients have included more realistic EOSs, magnetic fields and plasmas, and some simplistic treatments of neutrino and radiation physics. In this section, we review the more interesting developments relevant to astrophysics.

As in the case of binary black holes, several important qualitative questions about the merger process have been elucidated. The first relates to behavior postmerger and, for a sufficiently

massive remnant, the onset of collapse to a black hole. A large swath of parameters centered around the observationally favored initial neutron star masses of $\approx 1.4\,M_\odot$, and consistent with the highest-mass neutron stars observed to date ($\approx 2.\,M_\odot$; see Antoniadis et al. 2013 and Demorest et al. 2010 and related discussion by Lattimer & Prakash 2010), show an HMNS forms. From a fundamental gravity point of view, an interesting observation is that this intermediate state can have a highly dense central region and an effective angular momentum higher than the Kerr bound. Yet, obeying the cosmic censorship conjecture, the object does not evolve to a nakedly singular solution but is able to efficiently transport angular momentum outward to eventually allow a black hole to form. The black hole settles down to an approximate Kerr solution surrounded by some amount of material in a disk. A crucially important question then is, What is the timescale for collapse? This timescale depends sensitively on the initial conditions and several physical properties: the individual neutron star masses and eccentricity of the binary (which influences the initial distribution of mass among the HMNS and the bound and ejected material), the EOS, neutrino and photon cooling, and thermal pressure, as well as diverse mechanisms for angular momentum transport. The reason this is such an important question is that the timescale is in principle observable, either directly via the gravitational wave emission (as illustrated in **Figure 4**, though note that the frequency of the postmerger waves are sufficiently high that the adLIGO detectors will not be sensitive to them except for a highly unlikely nearby event) or indirectly through details of the counterpart electromagnetic/neutrino emission.

Beyond these broad qualitative issues, theoretical studies have been aimed to analyze in detail the coalescence process and characteristics of the gravitational wave emission. As mentioned, early stages of the dynamics are well captured by PN treatments. Approaching merger tidal effects do start to influence the evolution of the orbit, which would be reflected in the gravitational wave emission and could be detected via delicate data analysis (Hinderer et al. 2010; Damour, Nagar & Villain 2012). Another interesting premerger consequence of tidal forces during a quasi-circular inspiral is they can induce resonant oscillations in the interface modes (i-modes) between the neutron star crust and core that grow large enough to shatter the star's crust, leading to a potentially observable precursor electromagnetic outburst (Tsang et al. 2012). For highly eccentric close encounters, the tidal force is impulsive in nature. This can similarly shatter the crust (Tsang 2013) and will excite f-mode oscillations in the star (Stephens, East & Pretorius 2011; Gold et al. 2012). The f-modes do emit gravitational waves, though at frequencies that are too high and at amplitudes too weak for likely direct detection with adLIGO.

For low eccentricity encounters the stars merge at an orbital frequency that can be estimated by the point at which the stars come into contact, i.e., $\Omega_c \simeq [(m_1+m_2)(R_1+R_2)^3]^{1/2}$. At this stage, the stars are traveling at a considerable fraction ($\simeq$ 10–20%) of the speed of light, resulting in a violent collision. In the contact region, shock heating is responsible for a considerable amount of mass thrown outward (some of which becomes unbound) in a rather spheroidal shape. Also, strong shearing in this region induces Kelvin-Helmholtz instabilities, and strong differential rotation develops in the newly formed HMNS. The temperature of the HMNS can reach values of $\simeq$30–50 Mev, and magnetic fields can grow by several orders of magnitude [via winding, tapping kinetic energy, and possibly magnetorotational instabilities (MRIs), though for this latter process resolutions currently used are still far from that required to adequately resolve it]. Tidal tails form during the earlier stages of the merger and distribute material in the vicinity of the equatorial plane. As mentioned, because the total mass of the binary likely exceeds the maximum mass that a stable, nonrotating, and cold star might achieve, the subsequent behavior of the HMNS divides into two possible cases: prompt or delayed collapse.

In the prompt collapse case, thermal support and differential rotation are unable to overcome the gravitational attraction, and a black hole forms essentially in a free fall timescale. This takes

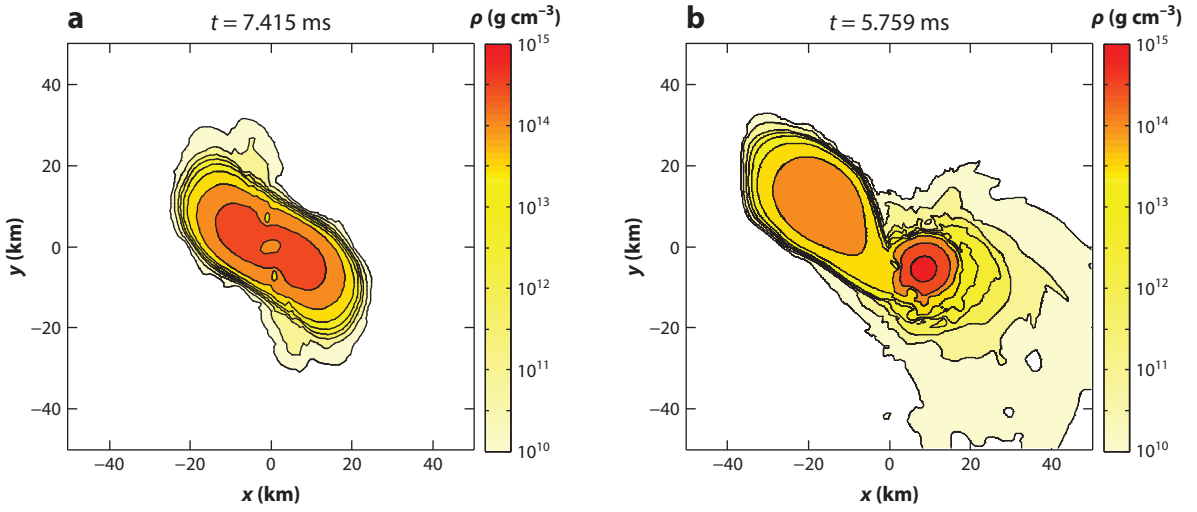

Figure 5

Equatorial density profiles ≃3 ms after merger from (*a*) an equal and (*b*) unequal mass binary neutron star system. Panel *a* corresponds to a system with $m_1 = m_2 = 1.643\,\mathrm{M}_\odot$ baryonic mass. Panel *b* corresponds to $m_1 = 1.304\,\mathrm{M}_\odot$ and $m_2 = 1.805\,\mathrm{M}_\odot$ baryonic masses. Reprinted from Rezzolla et al. (2010) with permission.

place in binaries with relatively large total mass $M_{\rm tot} \gtrsim 2.6$–$2.8\,\mathrm{M}_\odot$, though the exact value depends intimately on the EOS.

If the collapse does not occur promptly, the postmerger dynamics differ depending on whether the merger involved equal masses or not. If it is the former case, the newly formed object resembles a dumbbell composed of two cores (the remnants of the individual stars), which gradually turns into an ellipsoidal object as a result of angular momentum transport—primarily via hydrodynamics effects—and angular momentum loss via gravitational waves. For example, **Figure 5** illustrates the equatorial density of the remnant following an equal mass binary merger and another that had $m_1/m_2 = 0.7$. The gravitational waves from a postmerger system have a characteristic frequency in the range $2 \lesssim f \lesssim 4$ kHz which is proportional (and relatively close) to the Keplerian angular velocity $(M_{\rm HMNS}/R^3_{\rm HMNS})^{1/2}$ (where $M_{\rm HMNS}$, $R_{\rm HMNS}$ are the mass and radii of the HMNS, respectively). If the stars have different masses, the stronger tidal forces induced by the more massive star deforms the companion, stripping the outer layers and forming an envelope about the newly formed HMNS. This HMNS now displays two asymmetric cores and behaves as if the more massive core has a satellite that deforms dynamically as time progresses. Regardless of the mass ratio, a significant amount of material is estimated to lie beyond the ISCO of the black hole that will eventually form, resulting in an accretion disk with mass on the order of 0.01–$0.3\,\mathrm{M}_\odot$. Typically the more massive disks correlate with longer times to black hole formation, a behavior intuitively expected as there is more time for angular momentum to be transferred outward to the envelope.

Simulations have also shed light on the processes, and timescales, for such angular momentum transfer. The most important one is hydrodynamical, which begins to operate efficiently after the merger due to the strong torques induced by asymmetries in the HMNS. Other significant mechanisms for this transfer are tied to electromagnetic effects: winding and MRIs can do so by linking the central to outer regions of the HMNS and introducing an effective viscosity in the system. The angular momentum transport timescale due to winding is of the order of

$\tau_{\rm wind} \simeq R_{\rm HMNS}/v_{\rm A}$, with the Alfvén velocity $v_{\rm A} \simeq B/\sqrt{\rho}$. A few general relativistic simulations have pointed out that the strength of B can increase [in agreement with analogous results obtained in pseudo-Newtonian (Price & Rosswog 2006) or shearing box studies (Obergaulinger, Aloy & Müller 2010)] from typical premerger values of $10^{10-12}\,G$ to 10^{15-16} G via compression, winding, and transfer of hydrodynamical kinetic energy to electromagnetic energy via Kelvin-Helmholtz instabilities (Anderson et al. 2008b; Giacomazzo, Rezzolla & Baiotti 2011), which imply timescales $\tau_{\rm wind} \simeq 10$–$100$ ms. We stress, however, that present computational resources are still not adequate to give a thorough analysis of this process. For transport driven by the MRIs, simulations are even more challenging, so this is still a largely unexplored process within general relativistic simulations of binary neutron star mergers. Nevertheless, estimates indicate $\tau_{\rm MRI} \sim 100$ ms for putative magnetic field strengths of $B \simeq 10^{15}$ G. Therefore, either transport mechanism can operate on timescales $\gtrsim 10$–100 ms and aid in expediting the collapse. Cooling via neutrino and radiation transport reduces thermal-pressure support, so it also helps to shorten the time to collapse. However, the timescale for cooling to operate in a significant manner is on the order of seconds. Currently, simulations incorporating both electrodynamics and cooling are actively being pursued and refined.

Beyond the intricate details of the merger and postmerger behavior, there is strong interest in exploring binary neutron star mergers as progenitors of sGRBs and other electromagnetically observable signals. There is already tantalizing observational evidence for the connection between nonvacuum compact binaries mergers and sGRBs (see Berger 2014 for a recent review), strengthened by compelling theoretical models that suggest a merger yielding a rapidly accreting black hole could serve as the central energy source through hydrodynamical/plasma or neutrino processes (Eichler et al. 1989; Narayan, Paczynski & Piran 1992). Other models for the origin of at least a class of sGRBs include magnetars produced by binary neutron star mergers, binary white dwarf mergers or accretion-induced collapse of a white dwarf (Levan et al. 2006; Metzger, Quataert & Thompson 2008), and the collapse of an accreting neutron star to a black hole (MacFadyen, Ramirez-Ruiz & Zhang 2005). Simulations of these systems are providing valuable information to test these models. For instance, once collapse occurs, an initial hyperaccreting stage is observed, followed by a longer fall back accretion phase with the characteristic $t^{-5/3}$ power-law dependence expected from analytic calculations (Rees 1988). Beyond the burst itself, electromagnetic emission arising from the interaction of ejected material with the ambient medium, or through radioactive decay of r-process elements formed in this material shortly after merger, have been proposed (e.g., Metzger & Berger 2012; Piran, Nakar & Rosswog 2013). A candidate for this latter "kilonova" event has recently been observed (Berger, Fong & Chornock 2013; Tanvir et al. 2013). The timescale for this class of emission can be as long as days or weeks following merger, hence it is not amenable to ab initio simulations. However, results from simulations are consistent with properties assumed in these models to give observable signals; in particular, ejected material of order $\lesssim 10^{-4} M_{\rm eject}/{\rm M}_\odot \lesssim 10^{-2}$ traveling with velocities $\simeq 0.1$–$0.3c$ has been seen in noneccentric scenarios (with somewhat larger amounts/higher velocities possible in eccentric mergers). Finally, a magnetar with magnetic field strength likely in excess of 10^{15} G indeed forms during the merger of magnetized neutron stars, though its lifetime is typically $\lesssim 100$ ms except for the stiffest of EOSs and low-mass binaries (Anderson et al. 2008b; Giacomazzo, Rezzolla & Baiotti 2011). We conclude this section with a few miscellaneous topics related to binary neutron star mergers.

5.1.1. Magnetosphere interactions. Neutron stars have among the strongest magnetic fields in the Universe. As in the case of pulsars, they are surrounded by a magnetosphere that arises naturally as argued by Goldreich & Julian (1969). It is thus natural to expect that a binary interaction can trigger behavior related to that observed in pulsars (Lipunov & Panchenko 1996), though

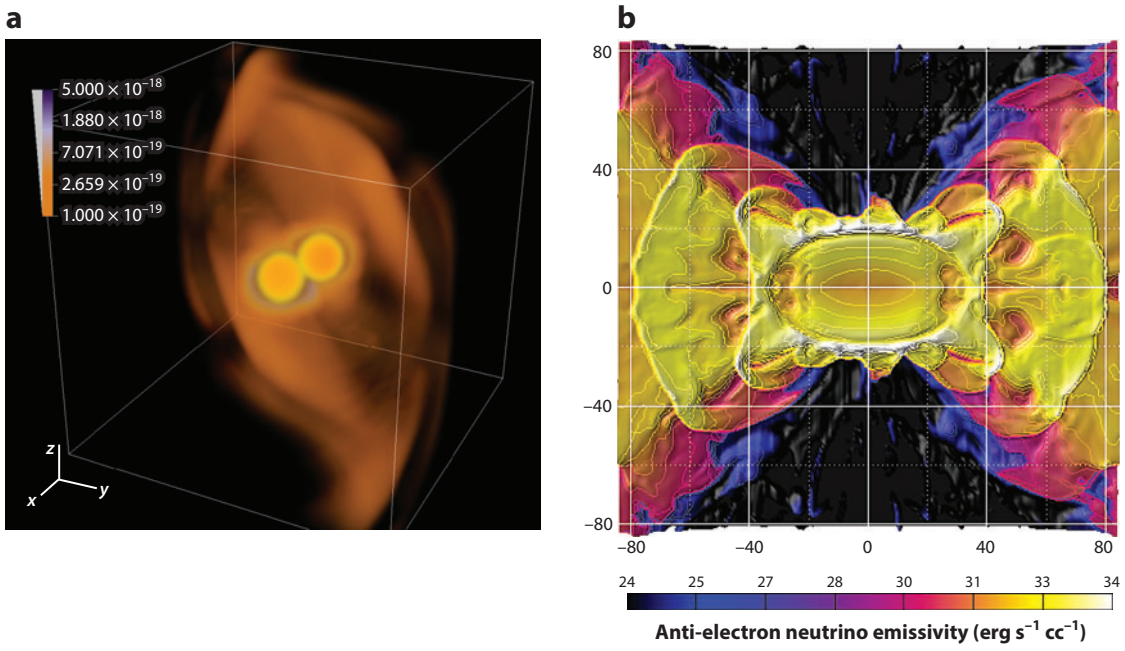

Figure 6

(*a*) Poynting flux produced by the magnetospheric interaction of orbiting, magnetized (with $B = 10^{12}$ G), equal-mass ($m_1 = m_2 = 1.4\,M_\odot$) neutron stars $\simeq$1.5 ms before merger. Reprinted from Palenzuela et al. (2013b) with permission. (*b*) Anti-electron neutrino luminosity in the *x*–*z* plane, 15 ms after an equal-mass ($m_1 = m_2 = 1.5\,M_\odot$) binary neutron star merger. Reprinted from Sekiguchi et al. (2011) with permission.

in this case with a tight connection to the orbital dynamics. This has recently been studied by Palenzuela et al. (2013a,b), showing that close to the merger event a strong Poynting flux is emitted ($L \simeq 10^{40-43}\,B_{11}^2$ erg s^{-1}); see **Figure 6*a*** for an illustration. As anticipated, many features common to those of pulsars are seen: the existence of gaps in the estimated charge density, shear layers, the development of a current sheet, and a striped structure in the toroidal magnetic field. In the binary case, however, these features bear tight imprints of the binary's behavior. For instance, as the orbit tightens, a ramp-up in Poynting luminosity ensues, and the current sheet structure displays a spiral pattern tied to the orbital evolution of the system. This could provide an important electromagnetic counterpart to the gravitational waves. In addition, the HMNS—which is likely highly magnetized as a result of the collision—can also trigger a strong Poynting flux as it collapses to a black hole (Lehner et al. 2012). The luminosity can be as large as $L \simeq 10^{49}(B/10^{15}\,G)^2$ erg s^{-1}, but shuts off abruptly as the black hole forms.

5.1.2. Neutrino emissions. Incipient works are beginning to incorporate estimates of neutrino effects in the system. This is because, as mentioned, the typical lifetime of the HMNS would likely be limited to $\lesssim$100 ms, whereas the timescale for neutrino cooling is on the order of seconds, as a first approximation a full (costly) radiation-transport scheme need not be employed. Instead, a simplified strategy known as a "leakage scheme" (Ruffert et al. 1997) has become the starting point. The leakage scheme ignores transport from the diffusion of neutrinos as well as neutrino momentum transfer. What it does model is the possible equilibration of neutrinos; it adopts an opaque, hot stellar matter model to describe local neutrino sources and sinks and

accounts for charged-current β processes, electron-positron pair-annihilation, and plasmon decays. At low optical depth the scheme uses reaction-rate calculations to estimate the local production and emission of neutrinos. In contrast, at high optical depths it assumes neutrinos are at their equilibrium abundances and that neutrino/energy losses occur at the diffusion timescale. In between, a suitable interpolation is adopted. Early efforts employing this scheme indicate a binary neutron star merger can produce strong neutrino luminosity of order $\simeq L_\nu \simeq 10^{54}$ erg s^{-1} (Sekiguchi et al. 2011). **Figure 6*b*** illustrates the antielectron neutrino luminosity shortly after an equal-mass ($m_1 = m_2 = 1.5\,\mathrm{M}_\odot$) merger.

5.1.3. Eccentric binaries. Binaries that emit observable gravitational waves while the orbit has high eccentricity show significant qualitative and quantitative differences in properties of the merger compared with equivalent-mass quasi-circular inspirals. Because there is more angular momentum in the binary when the two stars collide, typically more mass is stripped off, some fraction of which is ejected and the rest forms an accretion disk (East & Pretorius 2012, Gold et al. 2012). This has consequences for the magnitude of ejecta-powered counterparts, abundance of heavy elements produced through r-processes, and the range of initial neutron star masses that can lead to sufficiently massive disks to power an sGRB. The larger rotational energy also implies longer lifetimes for HMNS remnants. As mentioned above, close encounters prior to merger could induce sufficient strain in each neutron star to shatter its crust, leading to precursor electromagnetic emission (Tsang 2013). Furthermore, f-modes will be excited in each star. This changes the energetics of the orbit and indirectly affects the subsequent gravitational wave emission. The f-modes will also emit gravitational waves directly, though because of their relatively low amplitudes and high frequencies (around 1.5 kHz), they will not be observable with adLIGO-era detectors. Regarding the dominant emission from the orbital motion, as with eccentric binary black hole mergers, the challenge for detection is to construct waveform models accurate enough to use in template-based searches or devise alternative strategies (issues of rates aside). Also, even though the integrated energy released is order-of-magnitude comparable to a quasi-circular inspiral, more of it is radiated at higher frequencies in close periapse, high-eccentricity mergers. For a binary neutron star this occurs outside adLIGO's most sensitive range, making such a system unlikely to be detected beyond $\approx$50 Mpc even with matched filtering (East et al. 2013).

5.1.4. Alternative gravity theories. Binary neutron stars are also good candidates to test alternative theories of gravity, in particular those that predict deviations depending upon the coupling of matter to geometry. Scalar-tensor theories posit the existence of a scalar field that, together with geometry, mediates gravitational phenomena. A subclass of these theories allows a phenomenon known as *scalarization*, whereby a sufficiently compact star spontaneously develops a scalar charge that modifies its gravitational interaction with other stars and allows for dipole radiation from the system (Damour & Esposito-Farese 1992). Though observations of binary pulsar systems tightly constrain these theories (Antoniadis et al. 2013), recent numerical work has shown that within the allowable region of parameter space strong departures from general relativity can occur late in the inspiral (Barausse et al. 2013). These differences are triggered close to the merger epoch (yet while the gravitational wave frequencies are still well within the reach of near-future detectors) and significantly modify the dynamics, causing an earlier onset of the plunge (Barausse et al. 2013, Palenzuela et al. 2014, Shibata et al. 2014).

5.2. Black Hole–Neutron Star Mergers

The remaining binary that is a target for Earth-based gravitational wave detectors is composed of a black hole and a neutron star. Here again, the regime in which the objects are widely separated

is well described by a PN approximation, and the binary's dynamics proceeds as with the other cases discussed above. However, depending on the relation between two key radii—the tidal radius ($R_{\rm T}$) and the radius of the ISCO ($R_{\rm ISCO}$)—markedly different behavior is expected near merger. These radii, to leading order, depend on the black hole mass and spin (for $R_{\rm ISCO}$) as well as the binary-mass ratio, the star's mass, and EOS (for $R_{\rm T}$). Approximately, the tidal radius $R_{\rm T} \propto R_{\rm NS}(3M_{\rm BH}/M_{\rm NS})^{1/3}$; $R_{\rm ISCO}$ is $6M_{\rm BH}$ for a nonspinning black hole, decreasing (increasing) to $M_{\rm BH}$ ($9M_{\rm BH}$) for a prograde (retrograde) orbit about a maximally spinning Kerr black hole. The importance of these two radii stems from the intuition that a plunge precedes tidal disruption if $R_{\rm ISCO} > R_{\rm T}$, and the opposite otherwise. This distinction is crucial, as in the former case there would be little difference in the gravitational wave signal compared with a binary black hole merger having the same masses (Foucart et al. 2013). By contrast, if disruption occurs, at its onset gravitational wave emission is sharply suppressed, not only allowing differentiation from the binary black hole case but also presenting clues about the star's EOS as this influences the frequency at which the disruption takes place (for a given neutron star mass). It is easy to convince oneself that the disruption possibility favors high spins/comparable masses while the plunging behavior favors low spins/high mass ratios. Note also that there are fewer channels for electromagnetic emission if disruption does not occur; in particular sGRBs and kilonova require it.

These observations about the nature of black hole–neutron star mergers are clearly born out in simulations. Early studies began with polytropic EOSs and nonspinning black holes, which have steadily progressed to incorporate more realistic EOSs and have covered a fair range of mass ratios and black hole spins (Foucart 2012; Kyutoku, Ioka & Shibata 2013, 2014). New physics is also being modeled, as we discuss above with binary neutron stars (because, of course, the same code infrastructure is used for both). Nevertheless, the same caveats concerning neutron star–neutron star binaries apply to black hole–neutron star systems in that simulations have not yet covered the full range of possible parameters, nor are sufficient computational resources available at present to adequately model all the relevant scales and microphysics.

Regarding the systems in which $R_{\rm ISCO} < R_{\rm T}$ and disruption occurs, for quasi-circular mergers numerical simulations have found as much as $0.3\,{\rm M}_\odot$ of material outside the ISCO following merger (with the largest amounts coming from the low mass ratio/high prograde spin cases). These results have informed fitting formula predicting the amount of disk mass (Foucart 2012), which in turn can be used to estimate the spin of the final black hole (Pannarale 2014). Usually a larger fraction of stripped material is bound and subsequently accretes onto the black hole, though as much as $\approx 0.05\,{\rm M}_\odot$ can be ejected from the system, moving with speeds $\approx 0.2c$. Typical maximum temperatures following disruption reach $\simeq 80$ Mev. The tail regions are substantially cooler, at about $\simeq$10–100 Kev, though shocks can reheat this material to $\simeq$1–3 Mev. Interestingly, if the black hole spin and orbital angular momentum direction are misaligned, strong differences arise. For inclinations $\gtrsim 30°$ a very low-mass disk seems capable of forming, with most of the material outside $R_{\rm ISCO}$ and following highly eccentric trajectories having large semimajor axes (Foucart 2012; Kyutoku, Ioka & Shibata 2013, 2014). Based on these trajectories it is estimated this material will return to the black hole to accrete at a rate governed by the familiar law $\dot{M} \propto t^{-5/3}$ (Lee & Ramirez-Ruiz 2007, Chawla et al. 2010, Deaton et al. 2013). Interestingly, the behavior of this material has characteristics consistent with kilonova models. However, the ejecta distribution is mainly around the orbital plane as opposed to the rather spheroidal one arising in binary neutron star mergers. In many cases, the amount of material capable of forming a disk is consistent with estimates for triggering sGRBs.

At the other end of the spectrum with low spins and/or high mass ratios in which $R_{\rm T} < R_{\rm ISCO}$, the star plunges into the black hole with little or no material left behind. For low-spin black holes this outcome happens for $m_{\rm BH}/m_{\rm NS} \gtrsim 6$; higher spins (or eccentricity, discussed below) can push

this to somewhat larger mass ratios. For instance, for $m_{\rm BH} = 10\,{\rm M}_\odot$, $m_{\rm NS} = 1.4\,{\rm M}_\odot$, significant disruption only takes place for $a_{\rm BH}/m_{\rm BH} \gtrsim 0.9$ (Foucart et al. 2012). Without disruption, electromagnetic and neutrino counterparts such as sGRBs and kilonova are not expected to occur, though as we discuss below there may still be electromagnetic emission if the neutron star has a strong enough magnetic field. Naturally, as in the binary neutron star case, a plethora of phenomena can be triggered by the system's dynamics, and diverse works are proceeding to examine these scenarios, several of which we describe here.

5.2.1. Magnetized stars. A few studies have explored the behavior of the system when the neutron star is magnetized. Although electromagnetic effects are too subleading to alter the orbit and gravitational wave emission, the binary's dynamics can affect properties of the electromagnetic field after merger. In particular, the resulting field topology in the newly formed accretion disk is relevant to assessing whether a jet can be launched from the system. Notice that in the absence of spin-orbit-induced precession near the onset of disruption, the initial poloidal field gets twisted to a mainly toroidal configuration, implying further processes, such as dynamo/MRIs (Balbus & Hawley 1991), would need to take over to reinstate a poloidal configuration for an efficient jet mechanism to operate (McKinney & Blandford 2009). The orbit will precess if the black hole is spinning and the spin axis is misaligned with the orbital angular momentum; then the resulting magnetic field topology after disruption has both poloidal and toroidal components. This might aid in giving rise to favorable configurations for jet launching (see the discussion by Foucart 2012). Full simulations accurately resolving all of these effects for both precessing and nonprecessing configurations have yet to be performed, owing to their heavy computational requirements.

5.2.2. Magnetosphere interactions. As mentioned when discussing black holes interacting with a magnetosphere, the latter is able to tap kinetic energy—rotational or translational—from the black hole if there is a relative motion between them. Such a scenario naturally arises during the inspiral of a magnetized neutron star with a black hole (the binary will not be tidally locked, and so there will be relative motion of the black hole through the magnetic field lines sourced by the neutron star). Basic estimates using a simple "unipolar induction model" indicate the possibility of a strong Poynting luminosity produced by the system (Hansen & Lyutikov 2001, McWilliams & Levin 2011). First simulations in this direction have recently been completed, obtaining consistent values with $L \simeq 10^{41}\, B_{12}^2$ (Paschalidis, Etienne & Shapiro 2013). Though lacking a detailed account of how this Poynting flux could be converted to observable photons, this offers the possibility of an electromagnetic counterpart preceding the merger.

5.2.3. Neutrino emissions. As in the case of binary neutron stars, simulations are just beginning to incorporate neutrino effects, again using the leakage scheme. **Figure 7** shows an example of the neutrino luminosity from one such ongoing investigation (a follow-up study to Deaton et al. 2013). They found that the merger of a 1.4-$\rm M_\odot$ star with a black hole having mass $7\,{\rm M}_\odot$ and spin parameter $a/M \equiv J/M^2 = 0.9$ (so significant disruption takes place) yields a peak neutrino luminosity on the order of $\simeq 10^{54}$ erg $\rm s^{-1}$ shortly after disruption, decreasing by an order of magnitude after 50 ms.

5.2.4. Eccentric binaries. In eccentric black hole–neutron star encounters, similar quantitative and qualitative differences arise compared with quasi-circular inspiral as discussed above for the other systems (the possibility of zoom-whirl orbital dynamics, neutron star crust cracking, and/or excitation of f-modes during close encounters; typically larger amounts of ejecta and accretion disk mass; etc.). In addition, because the effective ISCO for eccentric orbits of particles orbiting

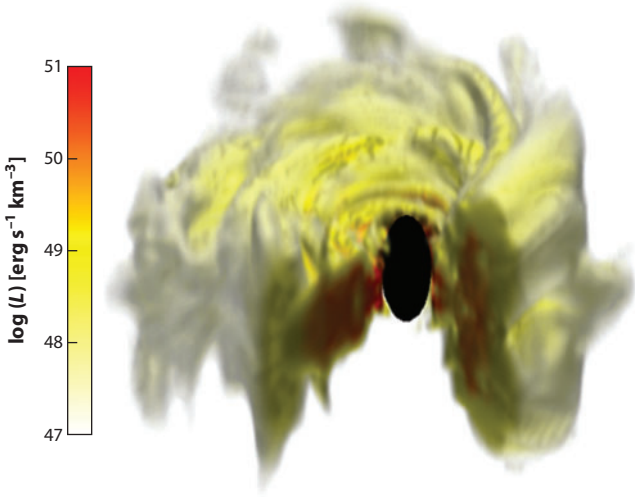

Figure 7

Luminosity from all neutrino species at ≃12.5 ms after the merger of a black hole ($M_{\rm BH} = 7\,{\rm M}_\odot$) with a neutron star ($M_{\rm NS} = 1.4\,{\rm M}_\odot$, described by the "LS220" equation of state). The emission region coincides roughly with the disk; namely densities $\rho > 3 \times 10^9$ g cm^{-3} are approximately within the white region, $\rho > 2 \times 10^{10}$ g c^{-3} the red/orange regions, and the maximum density in the disk is $\rho \simeq 6 \times 10^{11}$ g cm^{-3}. Figure from F. Foucart for the SXS Collaboration.

a nonextremal black hole is closer to the event horizon (e.g., for a Schwarzschild black hole the geodesic ISCO moves in from $r = 6M$ to $r = 4M$ going from $e = 0$ to 1), the limit for the onset of observable tidal disruption moves to slightly higher mass ratios. (Note by "observable" tidal disruption we mean disruption that can influence the gravitational waveform and the matter ejected or left to accrete. In theory the location of the event horizon sets the ultimate location for this, though for black hole–neutron star interactions the effective ISCO appears to be a better proxy. The reason is that once a matter parcel crosses the ISCO, barring the rise of strong nongravitational forces, it will reach the event horizon on the order of the time it takes light to cross the black hole. Though to date simulations have not included all the relevant matter microphysics, it is unlikely that effects triggered by tidal disruption, e.g., shock heating, shearing of magnetic fields, etc., could grow large enough on such a short timescale to prevent immediate accretion of the matter.) Furthermore, in systems where tidal disruption begins outside the ISCO there is the possibility of multiple partial disruptions and accretion episodes prior to the final disruption/merger (Stephens, East & Pretorius 2011, East, Pretorius & Stephens 2012a).

6. GRAVITATIONAL COLLAPSE TO A NEUTRON STAR OR BLACK HOLE

Considerable efforts have been undertaken to study gravitational collapse to a neutron star or a black hole, in particular within the context of core-collapse supernovae. Here, stars with masses in the range $10\,{\rm M}_\odot \lesssim M \lesssim 100\,{\rm M}_\odot$ at zero-age main sequence form cores that can exceed the Chandrasekhar mass and become gravitationally unstable. This leads to collapse that compresses the inner core to nuclear densities, at which point the full consequences of general relativity must be accounted for. Depending upon the mass of the core, it can "bounce" or collapse to a black hole. **Figure 8** displays representative snapshots of the behavior of a collapsing 75-$M_\odot$ star at

different times. The collapse forms a protoneutron star that later collapses to a black hole. In the case of a bounce, an outward propagating shock wave is launched that collides with still infalling material and stalls. Observations of core-collapse supernovae imply some mechanism is capable of reviving the shock, which is then able to plow through the stellar envelope and blow up the star. This process is extremely energetic, releasing energies on the order of 10^{53} erg, the majority of which is emitted in neutrinos (for a recent review, see Ott 2009). For several decades now, the primary motivation driving theoretical and numerical studies has been to understand what process (or combination of processes) mediates such revival and how. Several suspects have been identified: heating by neutrinos, (multidimensional) hydrodynamical instabilities, magnetic fields, and nuclear burning (see, e.g., Burrows et al. 2007, Janka et al. 2007). With the very disparate time- and space-scales involved, a multitude of physically relevant effects to consider, and the intrinsic cost to accurately model them (e.g., radiation transport is a seven-dimensional problem), progress has been slow. Moreover, electromagnetic observations do not provide much guidance to constrain possible mechanisms as they cannot peer deep into the central engine. In contrast, observations of gravitational waves and neutrinos have the potential to do so, provided the exploding star is sufficiently nearby. Thus, in addition to exploring mechanisms capable of reviving the stalled shock, simulations have also concentrated on predicting specific gravitational wave and neutrino signatures. Modeling gravity using full general relativity has only been undertaken recently (Ott et al. 2013), though prior to this some of the more relevant relativistic affects were incorporated (e.g., Dimmelmeier, Font & Müller 2002; Obergaulinger et al. 2006; Müller, Janka & Dimmelmeier 2010; Wongwathanarat, Janka & Mueller 2013). Although the full resolution of the problem is still likely years ahead, interesting insights into fundamental questions and observational prospects have been garnered. For example, simulations have shown that in rotating core-collapse scenarios, gravitational waves can be produced and their characteristics are strongly dependent on properties of the collapse: the precollapse central angular velocity, the development of nonaxisymmetric rotational instabilities, postbounce convective overturn, the standing accretion shock instability, protoneutron star pulsations, etc. If a black hole forms, gravitational wave emission is mainly determined by the quasi-normal modes of the newly formed black hole. The typical frequencies of gravitational radiation can lie in the range $\simeq$100–1,500 Hz and so are potential sources for advanced Earth-based gravitational wave detectors (though the amplitudes are sufficiently small that it would need to be a Galactic event). As mentioned, the characteristics of these waveforms depend on the details of the collapse and, hence, could allow us to distinguish the mechanism inducing the explosion. Neutrino signals have also been calculated, revealing possible correlations between oscillations of gravitational waves and variations in neutrino luminosities. However, current estimates suggest neutrino detections would be difficult for events taking place at kiloparsec distances (Ott et al. 2013).

7. FURTHER FRONTIERS

Beyond comparable-mass ratios and radii binaries, NR simulations are starting to explore binaries involving higher mass ratios or less dense stars: black hole–white dwarf, neutron star–white dwarf, intermediate mass black holes and main sequence stars, black hole binaries involving intermediate and stellar masses (Haas et al. 2012), etc. Here, more rapid progress is hampered by the computational cost, as it is considerably higher to simulate the larger range of spatial and temporal scales over which the interesting dynamics takes place. Several approaches have been suggested to address, at least in part, this difficulty. These include the use of implicit-explicit methods to tackle large-mass-ratio binary black holes (Lau, Lovelace & Pfeiffer 2011), a suitable rescaling of physical parameters to model neutron star–white dwarf binaries (Paschalidis et al. 2011), a "background

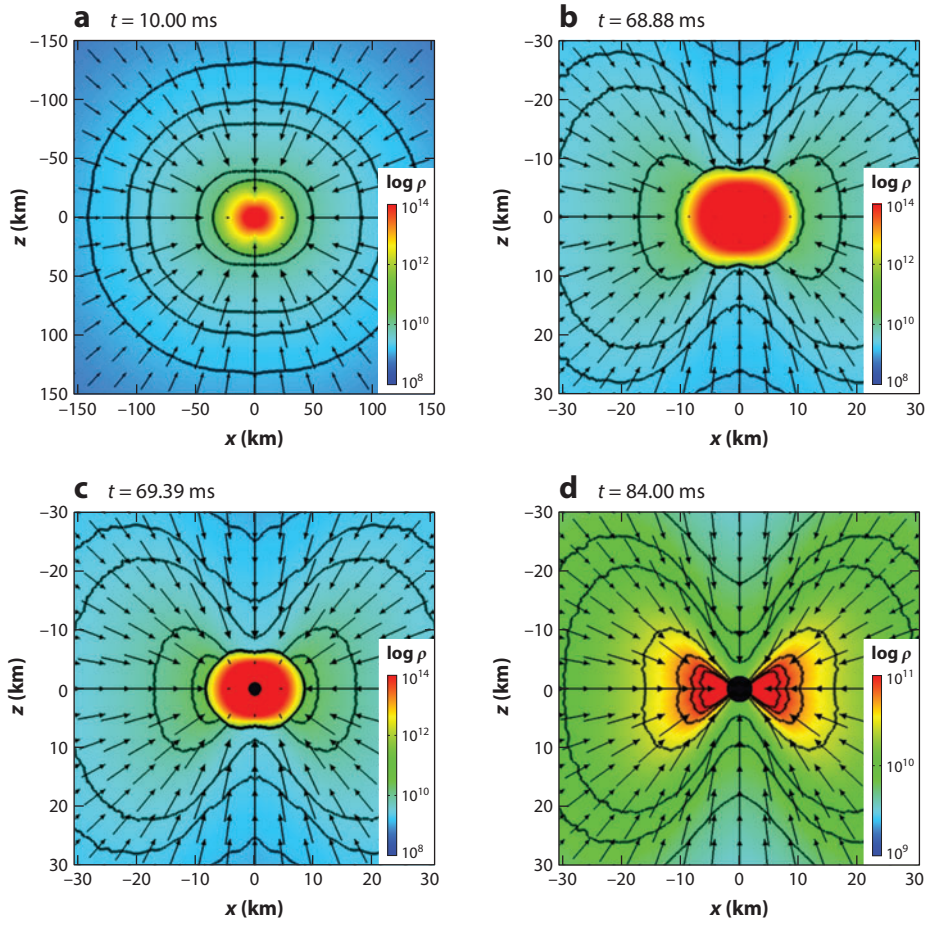

Figure 8

Density color maps of the meridional plane of a collapsing 75-$M_\odot$ star, superposed with velocity vectors at various times after bounce (and note the different scale of panel *a* from the rest). The collapse first forms (*a*,*b*) a protoneutron star that later collapses to (*c*,*d*) a black hole. Reprinted from Ott et al. (2011) with permission.

subtraction" technique to study extreme-mass-ratio systems in which the solution of the dominant gravitational body is known (East & Pretorius 2013), and a reformulation of the problem in terms of a PN approximation incorporating both black hole and matter effects to allow straightforward modification of existing "Newtonian-based" astrophysical codes (Barausse & Lehner 2013). These are illustrative examples indicating how the field is progressing beyond traditional boundaries. To date, however, as far as astrophysical applications are concerned, the predominant focus of NR has been the compact binary problem [and more recently including the study of core-collapse supernovae (Ott et al. 2013)]. Complementary efforts have been directed toward understanding fundamental questions about strongly gravitating settings, some of which have clear astrophysical implications. One example is the question of whether gravitational collapse always leads to a black hole, which is described by the Kerr solution, or to a naked singularity. Although the cases studied so far have indeed shown the black hole result to be the case, especially in astrophysically relevant contexts, counter examples have been constructed. In $d = 4$ spacetime dimensions these

include collapsing matter configurations finely tuned to the threshold of black hole formation [in so-called Type II critical collapse (Choptuik 1993); see, e.g., Gundlach (2003) for a review and Joshi (2013) for spherical collapse of ideal fluids]. Due to the fine tuning required to reach Planck-scale curvatures visible outside an event horizon, it is unlikely critical collapse occurs naturally in the Universe (though see Niemeyer & Jedamzik 1998 for arguments suggesting it would be relevant if certain primordial black hole formation scenarios occurred). By contrast, this is not the case in higher dimensions in which simulations of a class of black holes (black strings) have shown that violations of cosmic censorship can arise generically (Lehner & Pretorius 2010). This not only highlights that Einstein gravity still holds secrets that could be revealed by theoretical studies but also that surprises of astrophysical significance might be in store if our Universe were in fact higher dimensional.

8. FINAL COMMENTS

In this review, we have described the status of NR applied in astrophysical contexts. We have focused our presentation on events in which strong gravitational interactions require the full Einstein field equations to unravel all details of the phenomena. Due to page limitations, we have had to choose a representative subset of all relevant activities; nevertheless we hope it is clear that the field has "come of age." Yet there is still much to learn, and continued efforts will refine NR's predictions and application in astrophysics.

DISCLOSURE STATEMENT

The authors are not aware of any affiliations, memberships, funding, or financial holdings that might be perceived as affecting the objectivity of this review.

ACKNOWLEDGMENTS

We want to thank our collaborators on work mentioned here: M. Anderson, E. Barausse, W. East, E. Hirschman, S. Liebling, S. McWilliams, P. Motl, D. Neilsen, C. Palenzuela, F. Ramazanoglou, B. Stephens, and N. Yunes. We also acknowledge helpful discussions with K. Belczynski, E. Berger, D. Brown, A. Buonanno, C. Fryer, T. Janka, W. Lee, B. Metzger, R. Narayan, E. Poisson, E. Quataert, E. Ramirez-Ruiz, S. Rosswog, A. Spitkovsky, and J. Stone. For figures, we thank A. Buonanno, F. Foucart, B. Giacommazzo, R. Gold, M. Hannam, K. Hotokezaka, K. Kyutoku, C. Lousto, C. Ott, H. Pfeiffer, S. Shapiro, and M. Shibata. We also thank the participants of the "Chirps, Mergers and Explosions: The Final Moments of Coalescing Compact Binaries" workshop at the Kavli Institute for Theoretical Physics for stimulating discussions. This work was supported in part by an NSERC Discovery Grant and CIFAR (LL), NSF grants PHY-1065710 and PHY1305682, and the Simons Foundation (FP). Research at Perimeter Institute is supported by the Government of Canada through Industry Canada and by the Province of Ontario through the Ministry of Research and Innovation.

LITERATURE CITED

Abadie J, Abbott BP, Abbott R, Abernathy M, Accadia T, et al. 2010. *Class. Quant. Gravity* 27:173001
Abbott BP, Abbott R, Adhikari R, Ajith P, Allen B, et al. 2009. *Rep. Prog. Phys.* 72:076901
Accadia T, Acernese F, Antonucci F, Astone P, Ballardin G, et al. 2011. *Class. Quant. Gravity* 28:114002
Agathos M, Del Pozzo W, Li TGF, Broeck CVD, Veitch J, et al. 2014. *Phys. Rev. D* 89:082001

Ajith P, Hannam M, Husa S, Chen Y, Bruegmann B, et al. 2011. *Phys. Rev. Lett.* 106:241101
Alcubierre M. 2008. *Introduction to 3+1 Numerical Relativity*. Oxford, UK: Oxford Univ. Press
Amaro-Seoane P, Aoudia S, Babak S, Binetruy P, Berti E, et al. 2012. *GW Notes* 6:4-110
Anderson M, Hirschmann EW, Lehner L, Liebling SL, Motl PM, et al. 2008a. *Phys. Rev. D* 77:024006
Anderson M, Hirschmann EW, Lehner L, Liebling SL, Motl PM, et al. 2008b. *Phys. Rev. Lett.* 100:191101
Andersson N, Baker J, Belczynski K, Bernuzzi S, Berti E, et al. 2013. *Class. Quant. Gravity* 30:193002
Antognini JM, Shappee BJ, Thompson TA, Amaro-Seoane P. 2014. *MNRAS* 439(1):1079–91
Antoniadis J, Freire PCC, Wex N, Tauris TM, Lynch RS, et al. 2013. *Science* 340:448
Antonini F, Murray N, Mikkola S. 2014. *MNRAS* 439(1):1079–91
Arun KG, Iyer BR, Qusailah MSS, Sathyaprakash BS. 2006. *Class. Quant. Gravity* 23:L37–43
Baiotti L, Shibata M, Yamamoto T. 2010. *Phys. Rev. D* 82:064015
Baker JG, Centrella J, Choi D-I, Koppitz M, van Meter JR, Miller MC. 2006. *Ap. J. Lett.* 653:L93–96
Balbus SA, Hawley JF. 1991. *Ap. J.* 376:214–33
Barausse E. 2012. *MNRAS* 423:2533–57
Barausse E, Lehner L. 2013. *Phys. Rev. D* 88:024029
Barausse E, Morozova V, Rezzolla L. 2012. *Ap. J.* 758:63
Barausse E, Palenzuela C, Ponce M, Lehner L. 2013. *Phys. Rev. D* 87:081506
Barausse E, Rezzolla L. 2009. *Ap. J. Lett.* 704:L40–44
Baumgarte TW, Shapiro SL. 2010. *Numerical Relativity: Solving Einstein's Equations on the Computer*. Cambridge, UK: Cambridge Univ. Press
Berger E. 2014. *Annu. Rev. Astron. Astrophys.* 52:43–105
Berger E, Fong W, Chornock R. 2013. *Ap. J. Lett.* 774:L23
Berger MJ, Oliger J. 1984. *J. Comp. Phys.* 53:484
Berti E, Cardoso V, Gonzáles JA, Sperhake U, Hannam M, et al. 2007. *Phys. Rev. D* 76:064034
Berti E, Cardoso V, Starinets AO. 2009. *Class. Quant. Gravity* 26:163001
Berti E, Cardoso V, Will CM. 2006. *Phys. Rev. D* 73:064030
Berti E, Volonteri M. 2008. *Ap. J.* 684:822–28
Bini D, Damour T. 2012. *Phys. Rev. D* 86:124012
Blanchet L. 2002. *Living Rev. Relativ.* 5:3. **http://www.livingreviews.org/lrr-2002-3**
Blandford RD, Znajek RL. 1977. *MNRAS* 179:433–45
Bode T, Bogdanovic T, Haas R, Healy J, Laguna P, Shoemaker DM. 2012. *Ap. J.* 744:45
Bogdanovic T, Reynolds CS, Miller MC. 2007. *Ap. J. Lett.* 661:L147–50
Bona C, Bona-Casas C, Palenzuela-Luque C. 2009. In *Elements of Numerical Relativity and Relativistic Hydrodynamics*, ed. C Bona, C Palenzuela-Luque, C Bona-Casas. *Lect. Notes Phys.*, Vol. 783. Berlin: Springer-Verlag
Bower RG, Benson AJ, Malbon R, Helly JC, Frenk CS, et al. 2006. *MNRAS* 370:645–55
Boyd JP. 1989. *Chebyshev and Fourier Spectral Methods*. New York: Springer-Verlag
Boyle L, Kesden M, Nissanke S. 2008. *Phys. Rev. Lett.* 100:151101
Brodbeck O, Frittelli S, Hübner P, Reula OA. 1999. *J. Math. Phys.* 40:909–23
Broderick AE, Fish VL, Doeleman SS, Loeb A. 2011. *Ap. J.* 738:38
Broderick AE, Johannsen T, Loeb A, Psaltis D. 2014. *Ap. J.* 784:7–21
Broderick AE, Loeb A, Narayan R. 2009. *Ap. J.* 701:1357–66
Buonanno A. 2007. *Proc. Les Houches Summer Sch., Part. Phys. Cosmol.: Fabr. Spacetime, Les Houches, France*, Jul. 31–Aug. 25, 2006
Buonanno A, Cook GB, Pretorius F. 2007. *Phys. Rev. D* 75:124018
Buonanno A, Damour T. 1999. *Phys. Rev. D* 59:084006
Buonanno A, Kidder LE, Lehner L. 2008. *Phys. Rev. D* 77:026004
Burrows A, Dessart L, Ott CD, Livne E. 2007. *Phys. Rep.* 442:23–37
Campanelli M, Lousto CO, Zlochower Y, Merritt D. 2007. *Ap. J. Lett.* 659:L5–8
Casares J, Jonker P. 2014. *Space Sci. Rev.* In press. doi: 10.1007/s11214-013-0030-6
Centrella J, Baker JG, Kelly BJ, van Meter JR. 2010. *Annu. Rev. Nucl. Part. Sci.* 60:75–100
Chawla S, Anderson M, Besselman M, Lehner L, Liebling SL, et al. 2010. *Phys. Rev. Lett.* 105:111101
Choptuik MW. 1993. *Phys. Rev. Lett.* 70:9–12

Collins NA, Hughes SA. 2004. *Phys. Rev. D* 69:124022
Croton DJ, Springel V, White SDM, De Lucia G, Frenk CS, et al. 2006. *MNRAS* 365:11–28
Damour T, Esposito-Farese G. 1992. *Class. Quant. Gravity* 9:2093–176
Damour T, Nagar A, Bernuzzi S. 2013. *Phys. Rev. D* 87:084035
Damour T, Nagar A, Villain L. 2012. *Phys. Rev. D* 85:123007
Davis SW, Narayan R, Zhu Y, Barret D, Farrell SA, et al. 2011. *Ap. J.* 734:111
Deaton MB, Duez MD, Foucart F, O'Connor E, Ott CD, et al. 2013. *Ap. J.* 776:47
Demorest PB, Pennucci T, Ransom SM, Roberts MSE, Hessels JWT. 2010. *Nature* 467:1081–83
Dimmelmeier H, Font JA, Müller E. 2002. *Astron. Astrophys.* 388:917–35
Doeleman SS, Fish VL, Schenck DE, Beaudoin C, Blundell R, et al. 2012. *Science* 338:355
Dotti M, Volonteri M, Perego A, Colpi M, Ruszkowski M, Haardt F. 2010. *MNRAS* 402:682–90
Duez MD. 2010. *Class. Quant. Gravity* 27:114002
Duez MD, Foucart F, Kidder LE, Pfeiffer HP, Scheel MA, Teukolsky SA. 2008. *Phys. Rev.* D 78:104015
East WE, McWilliams ST, Levin J, Pretorius F. 2013. *Phys. Rev. D* 87:043004
East WE, Pretorius F. 2012. *Ap. J. Lett.* 760:L4
East WE, Pretorius F. 2013. *Phys. Rev. D* 87:101502
East WE, Pretorius F, Stephens BC. 2012a. *Phys. Rev. D* 85:124009
East WE, Pretorius F, Stephens BC. 2012b. *Phys. Rev. D* 85:124010
Eichler D, Livio M, Piran T, Schramm DN. 1989. *Nature* 340:126–28
Fanidakis N, Baugh CM, Benson AJ, Bower RG, Cole S, et al. 2011. *MNRAS* 410:53–74
Farrell S, Webb N, Barret D, Godet O, Rodrigues J. 2009. *Nature* 460:73–75
Farris BD, Gold R, Paschalidis V, Etienne ZB, Shapiro SL. 2012. *Phys. Rev. Lett.* 109:221102
Field SE, Galley CR, Herrmann F, Oschner E, Tiglio M. 2011. *Phys. Rev. Lett.* 106:221102
Flanagan EE, Hughes SA. 2005. *New J. Phys.* 7:204
Font JA. 2008. *Living Rev. Relativ.* 11:7
Foucart F. 2012. *Phys. Rev. D* 86:124007
Foucart F, Buchman L, Duez MD, Grudich M, Kidder LE, et al. 2013. *Phys. Rev. D* 88:064017
Foucart F, Duez MD, Kidder LE, Scheel MA, Szilagyi B, et al. 2012. *Phys. Rev. D* 85:044015
Garfinkle D, Lim WC, Pretorius F, Steinhardt PJ. 2008. *Phys. Rev. D* 78:083537
Gebhardt K, Kormendy J, Ho LC, Bender R, Bower G, et al. 2000. *Ap. J. Lett.* 543:L5–8
Gerosa D, Kesden M, Berti E, O'Shaughnessy R, Sperhake U. 2013. *Phys. Rev. D* 87:104028
Giacomazzo B, Rezzolla L, Baiotti L. 2011. *Phys. Rev. D* 83:044014
Godet O, Barret D, Webb N, Farrell S, Gehrels N. 2009. *Ap. J. Lett.* 705:L109–12
Gold R, Bernuzzi S, Thoerfelder M, Brügmann B, Pretorius F. 2012. *Phys. Rev. D* 86:121501
Gold R, Brügmann B. 2013. *Phys. Rev. D* 88:064051
Gold R, Paschalidis V, Etienne ZB, Shapiro SL, Pfeiffer HP. 2014. *Phys. Rev. D* 89(6):064060
Goldreich P, Julian WH. 1969. *Ap. J.* 157:869–80
González JA, Sperhake U, Brügmann B, Hannam MD, Husa S. 2007. *Phys. Rev. Lett.* 98:091101
Grandclement P, Novak J. 2009. *Living Rev. Relativ.* 12:1
Greene JE, Ho LC. 2004. *Ap. J.* 610:722–36
Gundlach C. 2003. *Phys. Rep.* 376:339–405
Gundlach C, Martin-Garcia JM, Calabrese G, Hinder I. 2005. *Class. Quant. Gravity* 22:3767–74
Gustafsson B, Kreiss HO, Oliger J. 1995. *Time Dependent Problems and Difference Methods*. New York: Wiley
Haas R, Shcherbakov RV, Bode T, Laguna P. 2012. *Ap. J.* 749:117
Hannam M. 2013. *Gen. Relativ. Gravit.* Accepted. arXiv:1312.3641
Hansen BM, Lyutikov M. 2001. *MNRAS* 322:695
Healy J, Levin J, Shoemaker D. 2009. *Phys. Rev. Lett.* 103:131101
Herrmann F, Hinder I, Shoemaker D, Laguna P. 2007. *Class. Quant. Gravity* 24:33
Hinder I, Buonanno A, Boyle M, Etienne ZB, Healy J, et al. 2013. *Class. Quant. Gravity* 31:025012
Hinderer T, Lackey BD, Lang RN, Read JS. 2010. *Phys. Rev. D* 81:123016
Horbatsch M, Burgess C. 2012. *J. Cosmol. Astropart. Phys.* 1205:010
Hotokezaka K, Kiuchi K, Kyutoku K, Muranushi T, Sekiguchi Y-I, et al. 2013. *Phys. Rev. D* 88:044026
Hughes S. 2009. *Annu. Rev. Astron. Astrophys.* 47:107–57

Int. Pulsar Timing Array. 2013. *Class. Quant. Gravity* 30:224010
Jacobson T, Sotiriou TP. 2009. *Phys. Rev. Lett.* 103:141101
Janka HT, Eberl T, Ruffert M, Fryer CL. 1999. *Ap. J. Lett.* 527:L39–42
Janka HT, Langanke J, Marek A, Martínez-Pinedo G, Müller B. 2007. *Phys. Rep.* 442:38–74
Johnson MC, Peiris HV, Lehner L. 2012. *Phys. Rev. D* 85:083516
Joshi PS. 2013. In *Spring Handbook of Spacetime*, ed. A Ashtekar, V Petkov. In press. New York: Springer arXiv:1311.0449
Kalogera V, Belczynski K, Kim C, O'Shaughnessy RW, Willems B. 2007. *Phys. Rep.* 442:75–108
Kamizasa N, Terashima Y, Awaki H. 2012. *Ap. J.* 751(1):39
Kaplan JD, Ott CD, O'Connor EP, Kiuchi K, Roberts L, Duez M. 2014. *Ap. J.* 790:19
Kesden M, Lockhart G, Phinney ES. 2010. *Phys. Rev. D* 82:124045
Kesden M, Sperhake U, Berti E. 2010. *Ap. J.* 715:1006–11
Kiuchi K, Sekiguchi Y, Kyutoku K, Shibata M. 2012. *Class. Quant. Gravity* 29:124003
Kocsis B, Levin J. 2012. *Phys. Rev. D* 85:123005
Komossa S. 2012. *Adv. Astron.* 2012:364973
Komossa S, Zhou H, Lu H. 2008. *Ap. J. Lett.* 678:L81–84
Kormendy J, Ho LC. 2013. *Annu. Rev. Astron. Astrophys.* 51:511–653
Kormendy J, Richstone D. 1995. *Annu. Rev. Astron. Astrophys.* 33:581
Kushnir D, Katz B, Dong S, Livne E, Fernández R. 2013. *Ap. J. Lett.* 778:L37
Kyutoku K, Ioka K, Shibata M. 2013. *Phys. Rev. D* 88:041503
Kyutoku K, Ioka K, Shibata M. 2014. *MNRAS* 437:L6
Laguna P, Garfinkle D. 1989. *Phys. Rev. D* 40:1011–16
Lattimer JM, Prakash M. 2010. In *From Nuclei to Stars*, ed. S Lee, p. 275. Singapore: World Sci.
Lau SR, Lovelace G, Pfeiffer HP. 2011. *Phys. Rev. D* 84:084023
Lee WH, Ramirez-Ruiz E. 2007. *New J. Phys.* 9:17
Lee WH, Ramirez-Ruiz E, Van de Ven G. 2010. *Ap. J.* 720:953
Lehner L. 2001. *Class. Quant. Gravity* 18:R25–86
Lehner L, Liebling SL, Reula OA. 2006. *Class. Quant. Gravity* 23:S421–46
Lehner L, Palenzuela C, Liebling SL, Thompson C, Hanna C. 2012. *Phys. Rev. D* 86:104035
Lehner L, Pretorius F. 2010. *Phys. Rev. Lett.* 105:101102
Lehner L, Reula O, Tiglio M. 2005. *Class. Quant. Gravity* 22:5283–322
Levan AJ, Wynn GA, Chapman R, Davies MB, King AR, et al. 2006. *MNRAS* 368:L1–5
LeVeque RJ. 1992. *Numerical Methods for Conservation Laws*. Basel: Birkhauser Verlag
Lippai Z, Frei Z, Haiman Z. 2008. *Ap. J. Lett.* 676:L5–8
Lipunov VM, Panchenko IE. 1996. *Astron. Astrophys.* 312:937–40
Loeb A. 2007. *Phys. Rev. Lett.* 99:041103
Löffler F, Faber J, Bentivegna E, Bode T, Diener P, et al. 2011. *Class. Quant. Gravity* 29:115001
Lousto CO, Campanelli M, Zlochower Y, Nakano H. 2010. *Class. Quant. Gravity* 27:114006
Lousto CO, Zlochower Y. 2011. *Phys. Rev. Lett.* 107:231102
Lousto CO, Zlochower Y, Dotti M, Volonteri M. 2012. *Phys. Rev. D* 85:084015
MacFadyen AI, Ramirez-Ruiz E, Zhang W. 2005. astro-ph/0510192
Magorrian J, Tremaine S, Richstone D, Bender R, Bower G, et al. 1998. *Astron. J.* 115:2285–305
McClintock JE, Narayan R, Davis SW, Gou L, Kulkarni A, et al. 2011. *Class. Quant. Gravity* 28:114009
McClintock JE, Narayan R, Steiner JF. 2013. *Space Sci. Rev.* In press. doi:10.1007/s11214-013-0003-9
McKinney JC, Blandford RD. 2009. *MNRAS* 394:L126–30
McWilliams ST, Levin JJ. 2011. *Ap. J.* 742:90
Metzger BD, Berger E. 2012. *Ap. J.* 746:48
Metzger BD, Quataert E, Thompson TA. 2008. *MNRAS* 385:1455–60
Milosavljević M, Phinney ES. 2005. *Ap. J. Lett.* 622:L93–96
Mösta P, Alic D, Rezzolla L, Zanotti O, Palenzuela C. 2012. *Ap. J. Lett.* 749:L32
Müller B, Janka HT, Dimmelmeier H. 2010. *Ap. J. Suppl. Ser.* 189:104–33
Narayan R, Paczynski B, Piran T. 1992. *Ap. J. Lett.* 395:L83
Neilsen D, Hirschmann EW, Millward RS. 2006. *Class. Quant. Gravity* 23:S505

Niemeyer JC, Jedamzik K. 1998. *Phys. Rev. Lett.* 80:5481–84
Noble SC, Mundim BC, Nakano H, Krolik JH, Campanelli M, et al. 2012. *Ap. J.* 755:51
Obergaulinger M, Aloy MA, Dimmelmeier H, Müller E. 2006. *Astron. Astrophys.* 457:209–22
Obergaulinger M, Aloy MA, Müller E. 2010. *Astron. Astrophys.* 515:A30
O'Leary RM, Kocsis B, Loeb A. 2009. *MNRAS* 395:2127–46
O'Shaughnessy R, Kaplan D, Sesana A, Kamble A. 2011. *Ap. J.* 743:136
Ott CD. 2009. *Class. Quant. Gravity* 26:063001
Ott CD, Abdikamalov E, Moesta P, Haas R, Drasco S, et al. 2013. *Ap. J.* 768:115
Ott CD, Reisswig C, Schnetter E, O'Connor E, Sperhake U, et al. 2011. *Phys. Rev. Lett.* 106:161103
Palenzuela C, Barausse E, Ponce M, Lehner L. 2014. *Phys. Rev. D* 89:044024
Palenzuela C, Garrett T, Lehner L, Liebling SL. 2010. *Phys. Rev. D* 82:044045
Palenzuela C, Lehner L, Liebling SL. 2010. *Science* 329:927–30
Palenzuela C, Lehner L, Liebling SL, Ponce M, Anderson M, et al. 2013a. *Phys. Rev. D* 88:043011
Palenzuela C, Lehner L, Ponce M, Liebling SL, Anderson M, et al. 2013b. *Phys. Rev. Lett.* 111:061105
Palenzuela C, Lehner L, Yoshida S. 2010. *Phys. Rev. D* 81:084007
Pan Y, Buonanno A, Taracchini A, Kidder LE, Mroué AH, et al. 2014. *Phys. Rev. D* 89:084006
Pannarale F. 2014. *Phys. Rev. D* 89:044045
Paschalidis V, Etienne ZB, Shapiro SL. 2013. *Phys. Rev. D* 88:021504
Paschalidis V, Liu YT, Etienne Z, Shapiro SL. 2011. *Phys. Rev. D* 84:104032
Peters PC. 1964. *Phys. Rev.* 136:B1224–32
Peters PC, Mathews J. 1963. *Phys. Rev.* 131:435–40
Peterson BM, Ferrarese L, Gilbert KM, Kaspi S, Malkan MA, et al. 2004. *Ap. J.* 613:682–99
Pfeiffer HP. 2012. *Class. Quant. Gravity* 29:124004
Piran T, Nakar E, Rosswog S. 2013. *MNRAS* 430:2121–36
Pretorius F. 2005. *Phys. Rev. Lett.* 95:121101
Pretorius F. 2006. *Class. Quant. Gravity* 23:S529–52
Pretorius F. 2009. In *Physics of Relativistic Objects in Compact Binaries: From Birth to Coalescence*, ed. M Colpi, P Casella, V Gorini, U Moschella, A Possenti, pp. 305–69. Heidelberg: Springer-Verlag
Pretorius F, Khurana D. 2007. *Class. Quant. Gravity* 24:S83–108
Price DJ, Rosswog S. 2006. *Science* 312:719–22
Read JS, Baiotti L, Creighton JDE, Friedman JL, Giacomazzo B, et al. 2013. *Phys. Rev. D* 88:044042
Rees MJ. 1988. *Nature* 333:523–28
Reynolds CS. 2013. *Class. Quant. Gravity* 30:244004
Rezzolla L, Baiotti L, Giacomazzo B, Link D, Font JA.2010. *Class. Quant. Gravity* 27:114105
Roedig C, Sesana A. 2012. *J. Phys. Conf. Ser.* 363:012035
Ruffert M, Janka HT, Takahashi K, Schäfer G. 1997. *Astron. Astrophys.* 319:122–53
Samsing J, MacLeod M, Ramirez-Ruiz E. 2014. *Ap. J.* 784:71
Sarbach O, Tiglio M. 2012. *Living Rev. Relativ.* 15:9
Scannapieco E, Silk J, Bouwens R. 2005. *Ap. J. Lett.* 635:L13–16
Scheel MA, Boyle M, Chu T, Kidder LE, Matthews KD, Pfeiffer HP. 2009. *Phys. Rev. D* 79:024003
Schmidt P, Hannam M, Husa S, Ajith P. 2011. *Phys. Rev. D* 84:024046
Schnetter E, Hawley SH, Hawke I. 2004. *Class. Quant. Gravity* 21:1465–88
Schnittman JD. 2013. *Class. Quant. Gravity* 30:244007
Sekiguchi Y, Kiuchi K, Kyutoku K, Shibata M. 2011. *Phys. Rev. Lett.* 107:051102
Seoane PA, Aoudia S, Audley H, Auger G, Babak S, et al. 2013. *The gravitational universe.* White Pap., The eLISA Space Gravitational Wave Observatory, Hanover, Ger. arXiv:1305.5720
Sesana A, Gair J, Berti E, Volonteri M. 2011. *Phys. Rev. D* 83:044036
Seto N. 2013. *Phys. Rev. Lett.* 111:061106
Shankar F. 2009. *New Astron. Rev.* 53:57–77
Shapiro SL. 2010. *Phys. Rev. D* 81:024019
Shapiro SL, Teukolsky SA. 1991. *Phys. Rev. Lett.* 66:994–97
Shibata M, Taniguchi K, Okawa H, Buonanno A. 2014. *Phys. Rev. D* 89(8):084005
Soltan A. 1982. *MNRAS* 200:115–22

Somiya K. 2012. *Class. Quant. Gravity* 29:124007
Stephens BC, East WE, Pretorius F. 2011. *Ap. J. Lett.* 737:L5
Stephens BC, Shapiro SL, Liu YT. 2008. *Phys. Rev. D* 77:044001
Stone N, Loeb A. 2011. *MNRAS* 412:75–80
Tanvir NR, Levan AJ, Fruchter AS, Hjorth J, Hounsell RA, et al. 2013. *Nature* 500:547–49
Taracchini A, Buonanno A, Pan Y, Hinderer T, Boyle M, et al. 2014. *Phys. Rev. D* 89:061502
Tchekhovskoy A, Narayan R, McKinney JC. 2010. *Ap. J.* 711:50–63
Tichy W, Marronetti P. 2008. *Phys. Rev. D* 78:081501
Tsang D. 2013. *Ap. J.* 777:103
Tsang D, Read JS, Hinderer T, Piro AL, Bondarescu R. 2012. *Phys. Rev. Lett.* 108:011102
Volonteri M, Sikora M, Lasota JP. 2007. *Ap. J.* 667:704–13
Volonteri M, Sikora M, Lasota JP, Merloni A. 2013. *Ap. J.* 775:94
Wainwright CL, Johnson MC, Peiris HV, Aguirre A, Lehner L, Liebling SL. 2014. *J. Cosmol. Astropart. Phys.* 1403:030
Wald RM. 1997. *Phys. Rev. D* 56:6467–74
Wen L. 2003. *Ap. J.* 598:419–30
Will CM. 1993. *Theory and Experiment in Gravitational Physics.* Cambridge, UK: Cambridge Univ. Press
Will CM. 2006. *Living Rev. Relativ.* 9:3. **http://www.livingreviews.org/lrr-2006-3**
Wongwathanarat A, Janka HT, Mueller E. 2013. *Astron. Astrophys.* 552:A126
Xue B, Garfinkle D, Pretorius F, Steinhardt PJ. 2013. *Phys. Rev. D* 88:083509
Yunes N, Pretorius F. 2009. *Phys. Rev. D* 80:122003